JGR Oceans

RESEARCH ARTICLE
10.1029/2021JC017525

Key Points:

- The first biogeochemical and spatial characterization of $\delta^{18}O$, δD, and $\delta^{13}C_{DIC}$ from coastal water masses in the Southeast Pacific (SEP)
- The upper 1,000 m between the open ocean and coastal regions show strong differences in water mass chemistry and geometry
- Coastal data provide information that can aid in reconstructions of past ocean conditions in the SEP

Supporting Information:

Supporting Information may be found in the online version of this article.

Correspondence to:

D. Reyes-Macaya,
dharmareyes@gmail.com

Citation:

Reyes-Macaya, D., Hoogakker, B., Martínez-Méndez, G., Llanillo, P. J., Grasse, P., Mohtadi, M., et al. (2022). Isotopic characterization of water masses in the Southeast Pacific region: Paleoceanographic implications. *Journal of Geophysical Research: Oceans*, *127*, e2021JC017525. https://doi.org/10.1029/2021JC017525

Received 3 MAY 2021
Accepted 2 DEC 2021

Author Contributions:

Conceptualization: Dharma Reyes-Macaya, Babette Hoogakker, Gema Martínez-Méndez, Mahyar Mohtadi, Dierk Hebbeln
Data curation: Dharma Reyes-Macaya, Pedro J. Llanillo, Patricia Grasse, Ricardo De Pol Holz, Cristian A. Vargas, Francisco García-Araya
Formal analysis: Dharma Reyes-Macaya, Alan Mix, Melanie J. Leng, Ulrich Struck, Daniel C. McCorkle, Macarena Troncoso, Carina B. Lange, Laura Farias,

Isotopic Characterization of Water Masses in the Southeast Pacific Region: Paleoceanographic Implications

Dharma Reyes-Macaya[1,2,3], Babette Hoogakker[2], Gema Martínez-Méndez[4], Pedro J. Llanillo[4], Patricia Grasse[5,6], Mahyar Mohtadi[1], Alan Mix[7], Melanie J. Leng[8,9], Ulrich Struck[10,11], Daniel C. McCorkle[12], Macarena Troncoso[13], Eugenia M. Gayo[3,13], Carina B. Lange[14,15,16,17,18], Laura Farias[3,13,15,19], Wilson Carhuapoma[20], Michelle Graco[20], Marcela Cornejo-D'Ottone[21,22], Ricardo De Pol Holz[23], Camila Fernandez[14,15,16,24,25], Diego Narvaez[14,15], Cristian A. Vargas[19,22,26], Francisco García-Araya[27], and Dierk Hebbeln[1]

[1]MARUM-Zentrum für Marine Umweltwissenschaften, Universität Bremen, Bremen, Germany, [2]Lyell Centre, Heriot-Watt University, Edinburgh, UK, [3]ANID-Millennium Science Initiative Program Nucleo Milenio UPWELL, La Serena, Chile, [4]AWI-Alfred Wegener-Institut Helmholtz-Zentrum für Polar- und Meeresforschung, Bremerhaven, Germany, [5]Deutsches Zentrum für Integrative Biodiversitätsforschung (iDiv), Halle-Jena-Leipzig, Germany, [6]GEOMAR-Helmholtz-Zentrum für Ozeanforschung, Kiel, Germany, [7]COAS-College of Earth, Ocean, and Atmospheric Sciences, Oregon State University, Corvallis, OR, USA, [8]National Environmental Isotope Facility, British Geological Survey, Nottingham, UK, [9]School of Biosciences, University of Nottingham, Loughborough, UK, [10]Museum für Naturkunde, Leibniz Institute for Evolution and Biodiversity Science, Berlin, Germany, [11]Department of Earth Sciences, Freie Universität Berlin, Berlin, Germany, [12]Woods Hole Oceanographic Institution, Falmouth, MA, USA, [13]ANID—FONDAP—Centro de Ciencia del Clima y Resiliencia, Universidad de Chile, Santiago, Chile, [14]Centro de Investigación Oceanográfica COPAS Sur-Austral, Universidad de Concepción, Concepción, Chile, [15]Departamento de Oceanografía, Universidad de Concepción, Concepción, Chile, [16]ANID—FONDAP—Centro IDEAL, Universidad Austral de Chile, Valdivia, Chile, [17]Scripps Institution of Oceanography, La Jolla, CA, USA, [18]Stazione Zoologica Anton Dohrn, Naples, Italy, [19]ANID-Millennium Science Initiative Program, Instituto Milenio en Socio-Ecología Costera, Santiago, Chile, [20]IMARPE-Instituto del Mar del Perú, Lima, Peru, [21]Escuela de Ciencias del Mar, Pontificia Universidad Católica de Valparaíso, Valparaíso, Chile, [22]ANID-Millennium Science Initiative Program, Instituto Milenio de Oceanografia, Concepción, Chile, [23]Centro de Investigación GAIA-Antártica and Network for Extreme Environment Research, Universidad de Magallanes, Punta Arenas, Chile, [24]Sorbonne Universités, UPMC University Paris 6, CNRS, Paris, France, [25]Laboratoire d'Océanographie Microbienne, Observatoire Océanologique de Banyuls sur Mer, Banyuls-sur-Mer, France, [26]Departamento de Sistemas Acuáticos, Facultad de Ciencias Ambientales, Universidad de Concepción, Concepción, Chile, [27]Departamento de Ciencias de la Tierra, Facultad de Ciencias Químicas, Universidad de Concepción, Concepción, Chile

Abstract In this study, we used stable isotopes of oxygen ($\delta^{18}O$), deuterium (δD), and dissolved inorganic carbon ($\delta^{13}C_{DIC}$) in combination with temperature, salinity, oxygen, and nutrient concentrations to characterize the coastal (71°–78°W) and an oceanic (82°–98°W) water masses (SAAW—Subantarctic Surface Water; STW—Subtropical Water; ESSW—Equatorial Subsurface water; AAIW—Antarctic Intermediate Water; PDW—Pacific Deep Water) of the Southeast Pacific (SEP). The results show that $\delta^{18}O$ and δD can be used to differentiate between SAAW-STW, SAAW-ESSW, and ESSW-AAIW. $\delta^{13}C_{DIC}$ signatures can be used to differentiate between STW-ESSW (oceanic section), SAAW-ESSW, ESSW-AAIW, and AAIW-PDW. Compared with the oceanic section, our new coastal section highlights differences in both the chemistry and geometry of water masses above 1,000 m. Previous paleoceanographic studies using marine sediments from the SEP continental margin used the present-day hydrological oceanic transect to compare against, as the coastal section was not sufficiently characterized. We suggest that our new results of the coastal section should be used for past characterizations of the SEP water masses that are usually based on continental margin sediment samples.

Plain Language Summary The Southeast Pacific (SEP) is a large marine region along the western continental margin of South America, where water masses that are transported from equatorial, subtropical, and subpolar latitudes converge. This study aims to understand the characteristics of water masses using isotopes of oxygen ($\delta^{18}O$), deuterium (δD), and dissolved inorganic carbon ($\delta^{13}C_{DIC}$) along with other parameters, such as temperature, salinity and oxygen, and nutrient concentrations. Significant differences in the chemical and isotope composition of SEP water masses are described. The distribution of the water masses above 1,000 m differs between our new coastal (71°–78°W) and partly existing oceanic (82°–98°W) sections. This

Wilson Carhuapoma, Michelle Graco, Marcela Cornejo-D'Ottone, Ricardo De Pol Holz, Camila Fernandez, Diego Narvaez, Francisco García-Araya
Funding acquisition: Dharma Reyes-Macaya, Babette Hoogakker, Mahyar Mohtadi, Carina B. Lange, Michelle Graco, Ricardo De Pol Holz, Dierk Hebbeln
Investigation: Dharma Reyes-Macaya, Babette Hoogakker, Gema Martínez-Méndez, Mahyar Mohtadi, Eugenia M. Gayo, Dierk Hebbeln
Methodology: Dharma Reyes-Macaya, Gema Martínez-Méndez, Pedro J. Llanillo, Patricia Grasse, Eugenia M. Gayo, Wilson Carhuapoma, Francisco García-Araya, Dierk Hebbeln
Project Administration: Dharma Reyes-Macaya, Dierk Hebbeln
Resources: Dharma Reyes-Macaya, Babette Hoogakker, Gema Martínez-Méndez, Carina B. Lange, Michelle Graco, Ricardo De Pol Holz, Camila Fernandez, Diego Narvaez, Dierk Hebbeln
Software: Dharma Reyes-Macaya, Pedro J. Llanillo, Francisco García-Araya
Supervision: Babette Hoogakker, Gema Martínez-Méndez, Mahyar Mohtadi, Dierk Hebbeln
Visualization: Dharma Reyes-Macaya, Francisco García-Araya
Writing – original draft: Dharma Reyes-Macaya, Babette Hoogakker, Gema Martínez-Méndez, Macarena Troncoso, Eugenia M. Gayo, Dierk Hebbeln
Writing – review & editing: Dharma Reyes-Macaya, Babette Hoogakker, Gema Martínez-Méndez, Pedro J. Llanillo, Patricia Grasse, Mahyar Mohtadi, Alan Mix, Melanie J. Leng, Ulrich Struck, Macarena Troncoso, Eugenia M. Gayo, Carina B. Lange, Laura Farias, Marcela Cornejo-D'Ottone, Ricardo De Pol Holz, Camila Fernandez, Diego Narvaez, Cristian A. Vargas, Dierk Hebbeln

has implications for the interpretation of paleoceanographic records, which are typically collected from the continental margin rather close to the coast.

1. Introduction

The coastal region of the Southeast Pacific (SEP) off Peru and Chile (as far as 38°S; Figure 1) hosts one of the most productive Eastern Boundary Current Upwelling Systems of the world (Chavez & Messié, 2009; Daneri et al., 2000; Montero et al., 2007). It has a complex water mass structure with a confluence of surface, subsurface and intermediate water masses coming from the subantarctic and the tropical Pacific, and recirculated deep waters (e.g., Silva et al., 2009; Strub et al., 1998). The interplay of these different waters plays a crucial role in the distribution of nutrients, heat, gases, and salt, which influence primary productivity, ocean circulation, and climate. Physical and chemical variables, such as temperature, salinity, and nutrients have been traditionally used to characterize water masses in the SEP (e.g., Llanillo et al., 2012, 2013; Silva et al., 2009). Since the WOCE program, several expeditions have taken place in offshore locations (oceanic region) of Peru and Chile. Among other measurements, seawater samples were collected and analyzed for their stable isotope composition to serve as a water mass tracers in the region. These tracers offered the opportunity to further improve our understanding of the complex physical processes affecting the water masses and biogeochemical cycles in the region (Druffel & Griffin, 2015; Kumamoto et al., 2011; Martínez-Méndez et al., 2013a; Quay et al., 2003).

Stable isotope ratios of oxygen ($\delta^{18}O$) and hydrogen (δD) in seawater have been used as a conservative hydrological tracers to determine the advection, mixing, and formation of water masses (Benway & Mix, 2004; Bigg & Rohling, 2000; Conroy et al., 2017; Craig & Gordon, 1965; LeGrande & Schmidt, 2006; Meredith et al., 1999; Schmidt, 1998, 1999). The $\delta^{18}O$ and δD values and their spatial distribution in the surface ocean are tied to the hydrological cycle through evaporation/precipitation (e.g., Conroy et al., 2013; Tiwari et al., 2013), atmospheric vapor transport (e.g., Benway & Mix, 2004), continental freshwater inputs (e.g., Khatiwala et al., 1999), and sea-ice formation/melting (e.g., Bass et al., 2014; Macdonald et al., 1999). Evaporation preferentially removes the lighter isotopes (^{16}O and ^{1}H) from the surface ocean layer, causing enrichment of the heavier isotopes (^{18}O and ^{2}H) as well as an increase in salinity. Precipitation and continental runoff/glacial-ice melting, return freshwater with lighter isotopes back to the ocean (Benway & Mix, 2004; Mackensen, 2001; Mikalsen & Sejrup, 2000). Hence, there are regional linear relationships between $\delta^{18}O$ and δD and salinity (conservative behavior; Benway & Mix, 2004; Bigg & Rohling, 2000; Conroy et al., 2017; LeGrande & Schmidt, 2006; Schmidt, 1998, 1999).

The stable carbon isotopic composition of dissolved inorganic carbon ($\delta^{13}C_{DIC}$) is a non-conservative tracer, and a semi-quantitative indicator of ventilation and water mass aging (Bostock et al., 2010, 2013; Kroopnick, 1985; Kumamoto et al., 2011). The distribution of $\delta^{13}C_{DIC}$ in the surface ocean is controlled by air-sea gas exchange, photosynthesis, carbonate precipitation, and ocean circulation (Gruber et al., 1999; McNeil et al., 2001). During photosynthesis, phytoplankton discriminates ^{12}C against ^{13}C, leaving seawater relatively enriched in ^{13}C leading to higher surface ocean $\delta^{13}C_{DIC}$ values, accompanied by low nutrient contents (Gruber et al., 1999). This relationship in surface waters is additionally affected by isotope fractionation that occurs during air-sea CO_2 exchange ($\delta^{13}C_{air\text{-}sea}$; Broecker & Maier-Reimer, 1992; Charles et al., 1993; Lynch-Stieglitz et al., 1995). For example, the cold temperatures in the surface layers in polar and subpolar regions increase the $\delta^{13}C_{air\text{-}sea}$ of water masses formed there and this isotopic signature is transferred to the ocean interior upon sinking and conserved until the water masses mix with other water masses (Bostock et al., 2010, 2013; Broecker & Maier-Reimer, 1992; Charles et al., 1993; Charles & Fairbanks, 1990; Oppo & Fairbanks, 1989). Furthermore, as particulate organic matter sinks into the deep ocean, aerobic and anaerobic remineralization within the water column releases ^{12}C and nutrients back to their dissolved inorganic forms ($\delta^{13}C_{bio}$). In combination with ocean circulation, $\delta^{13}C_{DIC}$ ($\delta^{13}C_{DIC} = \delta^{13}C_{air\text{-}sea} + \delta^{13}C_{bio}$) of ocean interior water masses become enriched in ^{12}C en route, a process called water mass "aging," making older waters carry lower $\delta^{13}C_{DIC}$ and higher nutrient contents (Kroopnick, 1985).

Understanding the distribution of $\delta^{13}C_{DIC}$, $\delta^{18}O$, and δD in the ocean is important since calcifiers (e.g., foraminifera) found buried in deep sea sediments as well as pore water/algae lipids, recording chemical signals, provide valuable information about past oceanographic environments and conditions.

The study of past water masses geometry and chemistry in the SEP, relies on downcore stable isotope records from calcifers collected from the shelf and slope of the western continental margin of South America. These allow the reconstructions of density, ventilation, oxygen, and nutrient contents in the water column on various time

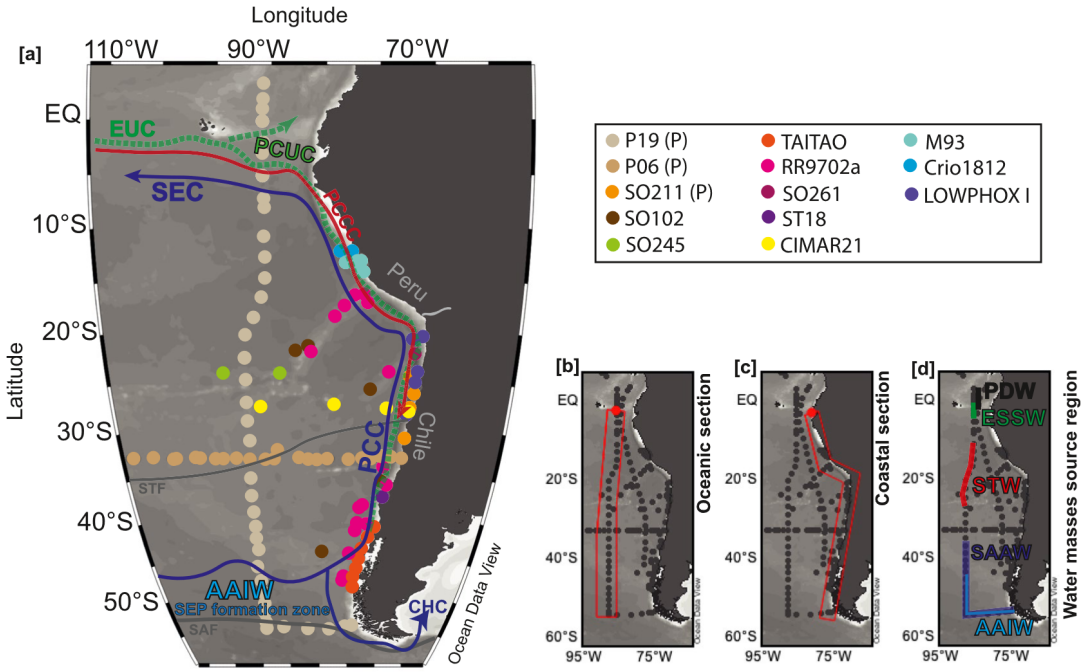

Figure 1. a) Location of the studied hydrological sites (colored dots refer to the individual expeditions listed in the inset and in Table 1). The red polygons in (b) and (c) indicate the meridional oceanic (on average > 1,000 km from the coast) and coastal (on average < 300 km from the coast) sections discussed in this study. Samples between the oceanic and coastal sections are not discussed in this study because they mostly comprise only surface waters and isolated samples from the water column. Features indicated in (a) are main ocean currents, oceanographic fronts, and the Antarctic Intermediate Water (AAIW) formation zone in the Southeast Pacific. Peru-Chile or Humboldt Current (PCC), Peru-Chile Counter Current (PCCC), Peru-Chile Undercurrent (PCUC), Equatorial Undercurrent (EUC), South Equatorial Current (SEC), Cape Horn Current (CHC), Subantarctic Front (SAF), and Subtropical Front (STF). In (d) the regions (colored) along the WOCE line P19, where the source water masses (Table 2) were defined are indicated. The stations of expeditions P19–P06 and SO211 correspond to published stable isotope data from the project GLODAP v2 https://www.glodap.info/ and Martinez-Mendez et al. (2013a), respectively.

scales (e.g., Haddam et al., 2018, 2020; Martínez-Fontaine et al., 2019; Martínez-Méndez et al., 2013a; Mohtadi et al., 2008; Nürnberg et al., 2015; Siani et al., 2013).

Most of the interpretations from past stable isotope records recovered from the continental shelf and slope in the SEP are based on comparisons with modern oceanographic data from the more oceanic part of the region. This may lead to biased interpretations. Some examples of potential biases are the over/underestimation of (a) changes in past water mass distribution and circulation, due to comparing the extension of a reconstructed water mass in the coastal section with its present extension in the more oceanic region (e.g., De Pol-Holz et al., 2006, 2007); (b) stable isotope disequilibria between water and calcite in proxy calibration studies, due to comparing the stable isotope signature of calcite of coastal samples with water samples collected in the oceanic section (Schmittner et al., 2017), and (c) traceability of regional isotope effects (e.g., biological and physical), which may explain the stable isotope signature of specific water masses (Mackensen, 2001).

Here, for the first time, we combine $\delta^{18}O$, δD, and $\delta^{13}C_{DIC}$ in seawater to characterize the SEP water masses, using published and new analyses from both the coastal and oceanic regions off Peru and Chile collected between 1992 and 2018. Our collection represents a time snapshot that includes potential seasonal, interannual, and decadal changes of the water masses; this long-term characterization will help to further understand the water masses and the processes, as well as providing calibrations for paleoceanography studies.

2. Regional Setting

2.1. Water Masses and Ocean Circulation

The SEP represents the ocean region from approximately the Equator to 53°S and between the western continental margin of South America and 90°W. It comprises the eastern part of the Equatorial Current System (with eastward and westward currents), eastern part of the South Pacific Subtropical Gyre (SPSG), the eastward West Wind Drift Current which comprises the Peru-Chile Current System (or Humboldt Current System) and the Cape Horn Current (Graco et al., 2013; Grados et al., 2018; Halpin et al., 2004; Stramma et al., 2010; Strub et al., 1998, 2019). Mesoscale surface and subsurface eddies are common, which act as efficient distributors of heat, salt, nutrients, and biomass to the open ocean (Cornejo D'Ottone et al., 2016; Hormazabal et al., 2013; Karstensen & Ulloa, 2009; Morales et al., 2012; Wang et al., 2018). Table S1 shows the acronyms for the individual currents and water masses addressed in this study.

The ocean and coastal regions off Chile and Peru are characterized by five main water masses: Subantarctic Surface Water (SAAW), Subtropical Water (STW), Equatorial Subsurface Water (ESSW), Antarctic Intermediate Water (AAIW), and Pacific Deep Water (PDW; Figures 1 and 2). At the surface, the relatively cold, fresh, oxygenated, $\delta^{13}C_{DIC}$ enriched, and low nutrient SAAW is advected equatorward from the Subantarctic Front (SAF) along the eastern part of the SPSG via the Peru-Chile Current (PCC) until ~32°S (Llanillo et al., 2012; Silva et al., 2009). SAAW flowing along the Chilean coast receives freshwater from perennial rivers and meltwater discharges from Patagonian fjords during austral summer (Silva et al., 1997) leading to a fresher SAAW variety (referred to Summer Subantarctic Surface Water, SSAAW; Llanillo et al., 2012). At the Subtropical Front (STF; 35°–30°S) the SAAW subducts into the ocean interior between 50 and 200 m; the subducted SAAW has been named the Eastern South Pacific Intermediate Water (ESPIW; Schneider et al., 2003).

North of 32°S, the surface ocean is occupied by the salty, warm, well-oxygenated STW, characterized by high values of $\delta^{13}C_{DIC}$ and low nutrient content. Most of the STW flows with the SPSG, but in the Tropical Eastern Pacific a fraction of STW is advected poleward by the Peru-Chile Counter Current (PCCC; Fiedler & Talley, 2006; Grados et al., 2018; Llanillo et al., 2012; Silva et al., 2009; Tsuchiya & Talley, 1998).

Between 200 and 600 m, the ESSW dominates the water column below the SAAW and STW in the tropical/subtropical SEP. This water mass is characterized by high salinity and nutrient contents, very low oxygen, and low $\delta^{13}C_{DIC}$ values (Garcia et al., 2014; Quay et al., 2003; Vargas et al., 2021; Wooster & Gilmartin, 1961). The ESSW derives from the mixing of aged water masses in the (western) Equatorial Pacific and is transported eastward by the Equatorial Undercurrent (EUC). Encountering the Galápagos Archipelago, the EUC deviates south into the SEP shadow zone, characterized by stagnant circulation, which enables further oxygen depletion in the ESSW (Strub et al., 1998). The ESSW is transported poleward along the continental slope by the Peru-Chile Undercurrent (PCUC; also known as the Gunther Undercurrent after Garcia et al., 2014; Llanillo et al., 2013; Wooster & Gilmartin, 1961). During upwelling events, the nutrient-rich ESSW reaches the surface ocean, and thus it is largely responsible for maintaining the high primary productivity and rich fisheries in the region (Montecino & Lange, 2009; Ulloa & Pantoja, 2009). This water mass is associated with the SEP oxygen minimum zone (SEP-OMZ; Silva et al., 2009) and is clearly identified from equatorial latitudes all the way south along the Chilean slope to temperate latitudes (38°S, Llanillo et al., 2012 and 48°S, Silva et al., 2009). Furthermore, south its low oxygen signature disappears through mixing with the SAAW and AAIW below.

At intermediate depths, between 500 and 1,000 m, the AAIW is characterized by relatively low salinity, temperature, and nutrient contents, and high levels of oxygen and $\delta^{13}C_{DIC}$ (Bostock et al., 2013; Hanawa & Talley, 2001; Martínez-Méndez et al., 2013a; Silva et al., 2009; Tsuchiya & Talley, 1998). One of the main source regions of AAIW today lies at Subantarctic latitudes close to Southern Patagonia (Hartin et al., 2011) from where the AAIW flows equatorwards at intermediate depths of the eastern boundary current, along the continental slope. Its influence remains still detectable in the equatorial region (Llanillo et al., 2013) albeit weak. AAIW is crucial for the ventilation of the thermocline and intermediate depths of the South Pacific Basin.

At depths >1,500 m, PDW dominates; it is characterized by high nutrient and low oxygen contents and low $\delta^{13}C_{DIC}$ values (Kumamoto et al., 2011). PDW is the most abundant and oldest water mass worldwide (DeVries, & Holzer, 2019; DeVries, & Primeau, 2011). It derives initially from a complex mixing of Lower Circumpolar Deep Water (LCDW), Antarctic Bottom Water (AABW) with SAAW, AAIW, and North Pacific Intermediate

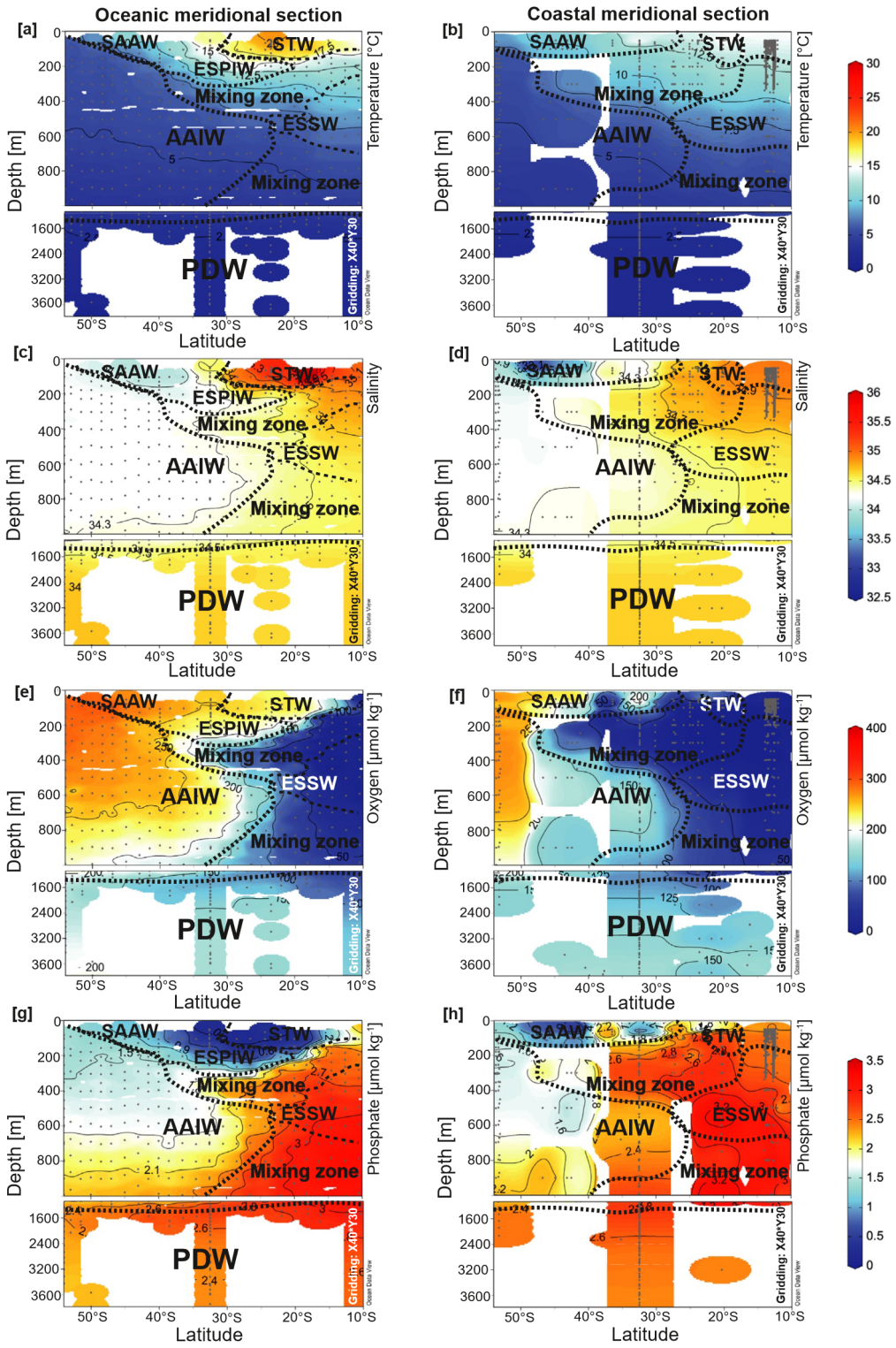

Figure 2. Hydrographic parameters: temperature (a and b), salinity (c and d), oxygen (e and f), phosphate (g and h) in the oceanic and coastal meridional section in the Southeast Pacific. Main water masses can be seen in all sections: SAAW (Subantarctic Surface Water), ESPIW (Eastern South Pacific Intermediate Water), STW (Subtropical Surface Water), ESSW (Equatorial Subsurface Water), AAIW (Antarctic Intermediate Water), and PDW (Pacific Deep Water). Each water sample site is represented by gray dots. The degree of gridding is indicated in the plot. Dashed lines represent the isoline of 50% of the contribution of the water mass to the water mixture. Grey dots show sample sites.

Water (Koshlyakov & Tarakanov, 2004). Along its very long path from high southern latitudes via the North Pacific and before returning south to the SEP, the PDW is further modified by mixing and geothermal warming (Talley, 2013).

Coupled ocean-atmosphere interannual and decadal-scale variations like the El Niño Southern Oscillation (ENSO) and the Pacific Decadal Oscillation (PDO) play a role in altering the mean distribution of the surface and intermediate waters in the SEP (Deutsch et al., 2011; Llanillo et al., 2013; Morales et al., 1999). Llanillo et al. (2013) show that during the warm phases of ENSO (El Niño) and PDO (El Viejo), the core of STW moves closer to the coast displacing ESSW downward and supplying the upper 250 m with oxygen. During the cold phases of ENSO (La Niña) and PDO (La Vieja) intensified upwelling increases the proportion of ESSW in shallower layers, enabling AAIW and ESPIW to concomitantly rise upward and reach further north thereby increasing the oxygenation of the lower part of the SEP-OMZ.

2.2. Upwelling Regime, Mesoscale Structures, and Primary Productivity

Along the western South American coast, the Southeast Pacific Subtropical Anticyclone (SPSA) drives upwelling favorable winds (Bakun & Nelson, 1991). Coastal upwelling causes upward advection of nutrient-rich ESSW, boosting high primary productivity up to ∼20 g C m^{-2} day^{-1} in the region (Daneri et al., 2000; Morales, Blanco, et al., 1996; Morales, Braun, et al., 1996; Testa et al., 2018).

The coastal upwelling regime has different spatial and temporal patterns along the western South American margin controlled by the SPSA, local topography, bathymetry, and water column stability (Figueroa & Moffat, 2000; Montecino et al., 2006). Upwelling is largely persistent between 12° and 24°S offshore Peru and northern Chile. However, between 17° and 20°S the Easterly Winds hit the land at a different angle than north or south of this location, therefore upwelling does not occur (e.g., ref. upwelling doldrum zone; Rutllant & Montecino, 2002). Toward the south, the upwelling regime changes from semi-permanent (23°S) to seasonal (33°–37°S; Letelier et al., 2009; Morales, Blanco, et al., 1996; Morales, Braun, et al., 1996). In this region, mesoscale eddies are often formed, changing the structure of the water column and regional biogeochemical cycles (Cornejo D'Ottone et al., 2016; Morales et al., 2012; Stramma et al., 2013).

In northern and southern Patagonia (>40°S) prevailing onshore Westerly winds together with the eastward directed Antarctic Circumpolar Current (Silva et al., 2009) promote downwelling (Shaffer et al., 1995; Strub et al., 1998). However, recent studies have shown that the upwelling/downwelling transition area off 40° and 42°S is shifting southward (Narváez et al., 2019).

Across these upwelling subsystems, maxima in primary productivity occur during austral spring and summer (Morales, Blanco, et al., 1996; Morales, Braun, et al., 1996). Between 30° and 38°S productivity is further fueled by nutrient inputs from river runoff (Masotti et al., 2018; Testa et al., 2018). High primary productivity along the Patagonian region is mainly supported by nutrient inputs brought about by localized rivers and glacier runoff (Pantoja et al., 2011).

3. Materials and Methods

3.1. Water Column CTD and Nutrient Data

In all expeditions (Table 1), Seabird-CTDs attached to Rosettes of Niskin bottles were used to measure conductivity, temperature, pressure, and oxygen. Nutrient samples were siphoned from Niskin bottles into 15 mL plastic vials, measured onboard or stored at −20°C for later measurements. The samples were measured using different autoanalyzer devices, depending on the expedition and laboratory (for further details see Table S2).

3.2. Extended Optimum Multi-Parameter Analysis

The Extended Optimum Multi-Parameter (EOMP) method was used to determine the water mass fractions (%) at each sampling point (Hupe & Karstensen, 2000; Karstensen & Tomczak, 1998). The EOMP is a multidimensional least-square fit that allows obtaining the percentage of mixing of more than three water masses in a water volume. The EOMP takes into consideration the biogeochemical cycling (respiration, remineralization, and denitrification) by including stoichiometry-scaled unknowns for the equation of each non-conservative parameter (Hupe

Table 1
Metadata of the Expeditions Providing the Sample Material and Data for This Study

Expedition ID	Research vessel ID	Sampling date (day/month/year)	Longitude ranges (degrees east)	Latitude ranges (degrees north)	Data provided by	Measurements
TAITAO	R/V Cabo de Hornos	01/11/2018 to 13/11/2018	−74.79 to −75.81	(−41.75) to (−47.66)	This study	$\delta^{13}C_{DIC}$, $\delta^{18}O$, δD, N, O_2, TSD
SO-261	R/V SONNE	06/03/2018 to 22/03/2018	(−70.88) to (−71.51)	(−21.82) to (−23.88)	This study	$\delta^{13}C_{DIC}$, $\delta^{18}O$, δD, O_2, TSD
SO-245	R/V SONNE	25/12/2015 to 30/12/2015	(−84.56) to (−90.03)	(−21.82) to (−23.88)	This study	$\delta^{13}C_{DIC}$, $\delta^{18}O$, δD, N*, O_2*, TSD*
316N138-3 (P06)	R/V Knorr	30/05/1992 to 06/06/1992	(−71.67) to (−96.67)	(−32.48) to (−32.51)	WOCE, 1992	$\delta^{13}C_{DIC}$*, N*, O_2*, TSD*
49NZ20030909 (P06)	R/V Mirai	03/08/2003 to 16/10/2003	(−72.71) to (−98.66)	(−32.49) to (−32.50)	WOCE, 2003	$\delta^{13}C_{DIC}$*, N*, O_2*, TSD*
318M20100105 (P06)	R/V Melville	05/01/2010 to 1/02/2010	(−71.92) to (−100.56)	(−32.49) to (−32.50)	WOCE, 2010	$\delta^{13}C_{DIC}$*, N*, O_2*, TSD*
LOWPHOX 1	R/V Cabo de Hornos	11–12/2015	(−70.51) to (−71.34)	(−20.1) to (27.66)	This study	$\delta^{13}C_{DIC}$, $\delta^{18}O$, N, O_2, TSD
RR9702a	R/V Roger Revelle	2–4/1997	(−73) to (−81.5)	(−13.70) to (−47)	This study	$\delta^{13}C_{DIC}$, O_2
SO-102	R/V SONNE	09/05/1995 to 28/06/1995	(−72.81) to (−82.91)	(−21.08) to (−43.24)	This study	$\delta^{13}C_{DIC}$, N, O_2, TSD
SO-211	R/V SONNE	10/11/2010 to 26/11/2010	(−70.65) to (−71.77)	(−23.85) to (−30.24)	This study	$\delta^{13}C_{DIC}$*, $\delta^{18}O$, O_2, TSD
Station18-Udec	L/C Kay Kay II	19/05/2015 and 23/06/2015	−73	−36.50	This study	$\delta^{13}C_{DIC}$, $\delta^{18}O$, N, O_2, TSD
CIMAR-21	R/V Cabo de Hornos	12/10/2015 to 20/10/2015	(−71.25) to (86.8)	(−27.09) to (−27.24)	This study	$\delta^{13}C_{DIC}$, $\delta^{18}O$, N**, O_2**, TSD**
Crio1812	R/V Jose Oyala	27/12/2018 to 28/12/2018	(−77.22) to (−78.85)	−12	This study	$\delta^{13}C_{DIC}$, $\delta^{18}O$, δD, N, O_2, TSD
316N138_12 (P19)	R/V Knorr	22/02/1993 to 13/04/1993	(−75.02) to (−88)	(−8) to (−54)	WOCE, 1993	$\delta^{13}C_{DIC}$*, N*, O_2*, TSD*
M93	R/V Meteor	06/02/2013 to 10/03/2013	(−76) to (−78)	(−12) to (−13)	This study	$\delta^{13}C_{DIC}$, N*, O_2*, TSD*

Note. Type of data and samples obtained per expedition are indicated in Tables S1–S3. N: Nutrients; TDS: Temperature, salinity, and density. * SO245 (Ferdelman et al., 2019), SO211 (Martínez-Méndez et al., 2013b, 2013c, 2013d, 2013e), M93 (Lavik & Krahmann, 2016). **CIMAR21 data set from shallow water depth is available in Farías and Troncoso (2021), in this study we add information about deep stations. * and ** data sets are available in GLODAP and PANGAEA webpages.

& Karstensen, 2000). The parameters used for the EOMP analysis are potential temperature, salinity, oxygen, and inorganic nutrients (phosphate, silicate, and nitrate; Hupe & Karstensen, 2000; Karstensen & Tomczak, 1998; Poole & Tomczak, 1999). The EOMP analysis requires a correct definition of the source water masses expected to contribute to the observed parameter in the water mixture. The source regions (Figure 1c) for the five main water masses addressed in this study are summarized in Section 2.1 (Table 1).

We used the potential temperature, salinity, oxygen, silicate, and nitrate end-members calculated for SAAW, STW, ESSW, AAIW, and PDW by Llanillo et al. (2013; Table 2) assuming that the source waters are in a theoretical steady state. Hence, changes in the water mass fractions and their biogeochemical signals are interpreted as responding solely to the redistribution of water masses and to different biogeochemical cycling (remineralization and denitrification).

Before resolving the EOMP, the different parameters are normalized and weighted in order to control their relative influence on the solution (Tomczak & Large, 1989). The largest weights are assigned to mass conservation (i.e., the mass conservation equation will be more relevant for the resolution of the EOMP) and to the parameters with the largest sampling accuracy (potential temperature and salinity). For potential temperature and salinity the assigned weight was 24. Nutrients, such as phosphate, nitrate, and nitrite have weights of 7. Due to a non-constant

Table 2
Southeast Pacific Source Water Mass Types (Figure 1d) Used for the EOMP Analysis to Obtain $\delta^{13}C_{DIC}$, $\delta^{18}O$, and δD End-Members

Water mass	Pot. Temp. (°C)	Salinity	Oxygen (μmol kg^{-1})	Phosphate (μmol kg^{-1})	Silicate (μmol kg^{-1})	Nitrate (μmol kg^{-1})	$\delta^{13}C_{DIC}$ (‰)	$\delta^{18}O$ (‰)	δD (‰)
STW	20.80	35.52	240.65	0.46	2.23	0.74	0.42	0.60	3.22
SAAW	11	34	268.20	1.07	2.17	13.70	1.81	−0.12	−1.17
ESSW	10	34.80	13.60	2.43	29.81	32.70	−0.48	0.31	0.82
AAIW	3.00	34	238.20	1.97	24.60	28.50	1.59	0.00	−1.01
PDW	1.82	34.67	105.20	2.76	157.30	38.42	0.04	0.01	−1.28
Weight	24	24	7	7	3.5	7	–	–	–

Note. The source water masses are Subtropical Surface Water (STW), Subantarctic Surface Water (SAAW), Equatorial Subsurface Water (ESSW), Antarctic Intermediate Water (AAIW), and Pacific Deep Water (PDW). The water type values and weights (bottom row) of potential temperature, salinity, oxygen, phosphate, silicate, and nitrate concentrations were obtained from Llanillo et al. (2013). The variables considered conservative are potential temperature, salinity, $\delta^{18}O$, and δD. Oxygen, phosphate, silicate, nitrate, and $\delta^{13}C_{DIC}$ parameters were considered non-conservative.

relationship during remineralization with phosphate and nitrate, silicate was assigned with half of the nutrient weight (3.5; Llanillo et al., 2013; Table 2).

The EOMP analysis was applied to the full data set including the oceanic and coastal hydrological sections (Figure 1), excluding those data points located within the uppermost 55 m of the water column that correspond to an average mixed layer estimated for the study area (Leth et al., 2004; Llanillo et al., 2013). As mixed layer points are influenced by air-sea interaction processes, they cannot be resolved with the EOMP (i.e., potential temperature and salinity are not conservative).

Only data points with a mass conservation error <4% were selected for this study and, consequently, this can be interpreted as the uncertainty associated with the EOMP results. In 1,094 out of 2,680 data points it was possible to apply the EOMP analysis. 40% of the data qualify for EOMP analyses, providing new insights into the oceanography of this region with the largest dataset for the SEP so far.

3.3. Water Column Stable Isotope Data

Water samples for $\delta^{18}O$, δD, and $\delta^{13}C_{DIC}$ were collected during several expeditions conducted between 1992 and 2018 in the SEP using Niskin bottles coupled in a Rosette with CTD device (see Table S3 and S4). The RR-9702a expedition is an exception; a single Niskin bottle was coupled to the top of a multicorer device. To prevent contamination and/or micro-evaporation, water samples were immediately siphoned from Niskin bottles into 100 and 25 mL glass and polypropylene bottles avoiding bubbles. Water samples for $\delta^{13}C_{DIC}$ determinations were poisoned onboard with 0.5 mL of ultra-saturated mercury chloride ($HgCl_2$) to avoid alternating the $\delta^{13}C_{DIC}$ signature by further remineralization. All $\delta^{18}O$, δD, and $\delta^{13}C_{DIC}$ samples were sealed with parafilm and kept at 4°C until analysis in the laboratory.

3.3.1. Water Column $\delta^{18}O$ and δD Analyses

The $\delta^{18}O$ ($n = 200$, 8 expeditions) and δD ($n = 90$, 8 expeditions) compositions of water samples were determined at MARUM-Bremen, CEOAS-Oregon, and BGS-Nottingham laboratories (see Tables 1 and S3). At MARUM-Bremen, dual $\delta^{18}O$-δD analyses were conducted using a Picarro L-2130i performing nine injections per sample. The first seven injections were ignored to preclude memory effects that potentially might occur in continuous runs of several samples. Results obtained were normalized to VSMOW2 through repeated analyses of house standards as SLAP2 (Standard Light Antarctic Precipitation 2; $\delta^{18}O$: −55.5 ± 0.02‰, δD: −427.5 ± 0.3‰; IAEA, 2017) and VSMOW2 (Vienna Standard Mean Ocean Water; $\delta^{18}O$: 0 ± 0.02‰, δD: 0 ± 0.3‰; IAEA, 2017). Measurement errors for all samples were about 0.08‰ for $\delta^{18}O$ and 0.2‰ for δD.

At CEOAS-Oregon and BGS-Nottingham $\delta^{18}O$ analyses were done by isotope ratio (dual inlet) mass spectrometry using a DeltaPlus X and Isoprime 100 mass spectrometer plus Aquaprep device, respectively. Both

Table 3
Mean and Standard Deviation ($\mu \pm 1\sigma$) in the 50% Contribution Isoline of Each Main Water Mass to the Water Mixture in the Coastal and Ocean Section

Water mass	Temperature (°C)	Salinity	Oxygen (μmol kg^{-1})	Silicate (μmol kg^{-1})	Phosphate (μmol kg^{-1})	Nitrate (μmol kg^{-1})	Nitrite (μmol kg^{-1})	$\delta^{18}O$ (‰)	δD (‰)	$\delta^{13}C_{DIC}$ (‰)	$\delta^{13}C_{air\text{-}sea}$ (‰)
STW coast	14.03 ± 1.18	34.93 ± 0.08	11.20 ± 9.93	22.73 ± 5.20	2.67 ± 0.47	16.85 ± 6.82	1.34 ± 2.13	0.32 ± 0.17	1.61 ± 0.12	−0.41 ± 0.32	0.04 ± 0.48
STW ocean	17.47 ± 1.08	35.11 ± 0.19	207.17 ± 56.03	3.33 ± 3.62	0.64 ± 0.54	4.78 ± 7.72	0.13 ± 0.26	–	–	1.59 ± 0.46	−0.43 ± 0.14
SAAW coast	10.97 ± 1.75	34.10 ± 0.21	190.73 ± 56.93	5.12 ± 4.43	1.34 ± 0.51	14.40 ± 6.38	0.12 ± 0.11	−0.10 ± 0.25	−0.13 ± 0.39	1.16 ± 0.46	−0.03 ± 0.37
SAAW ocean	11.63 ± 2.36	34.28 ± 0.19	229.62 ± 38.07	2.87 ± 2.12	1.00 ± 0.39	11.85 ± 5.98	0.12 ± 0.19	–	–	1.48 ± 0.26	−0.08 ± 0.33
ESSW coast	10.87 ± 2.27	34.74 ± 0.19	18.64 ± 26.58	25.44 ± 5.87	2.57 ± 0.30	25.94 ± 7.91	2.15 ± 2.29	0.30 ± 0.25	1 ± 0.79	−0.07 ± 0.31	0.52 ± 0.12
ESSW ocean	9.8 ± 2.22	34.70 ± 0.16	24.54 ± 30.67	34.68 ± 12.30	2.65 ± 0.33	34.97 ± 5.50	0.01 ± 0.03	–	–	0.19 ± 0.23	0.32 ± 0.35
AAIW coast	5.05 ± 0.74	34.26 ± 0.08	212.81 ± 54.27	19.82 ± 11.24	1.97 ± 0.34	27.53 ± 5.57	0.04 ± 0.09	−0.02 ± 0.16	−0.55 ± 0.58	1.01 ± 0.29	0.54 ± 0.28
AAIW ocean	5.23 ± 0.92	34.26 ± 0.05	241.16 ± 43.62	17.47 ± 11.14	1.82 ± 0.31	26.03 ± 4.61	0.02 ± 0.08	–	–	1.14 ± 0.30	0.53 ± 0.17
PDW coast	2.24 ± 0.54	34.63 ± 0.06	140.17 ± 20.34	112.05 ± 17.01	2.57 ± 0.14	36.36 ± 2.10	0.01 ± 0.02	–	–	0.20 ± 0.09	0.43 ± 0.23
PDW ocean	2.86 ± 0.82	35.59 ± 0.07	120.75 ± 39.09	103.79 ± 22.95	2.70 ± 0.26	38.06 ± 2.95	0.00 ± 0.00	–	–	0.19 ± 0.20	0.44 ± 0.22

Note. For $\delta^{18}O$ and δD in the water masses from the oceanic section and for the PDW in the coastal section the data was not sufficient for the analysis.

laboratories followed the water-CO_2 equilibration method modified by Epstein and Mayeda (1953). Working standards SLAP2 and GISP (Greenland Ice Sheet Precipitation; $\delta^{18}O$: −24.76 ± 0.09‰, δD: −189.5 ± 1.2‰, IAEA, 2017) indicate measurement errors at <0.05‰ for $\delta^{18}O$ and the results were corrected to VSMOW.

3.3.2. Water Column $\delta^{13}C_{DIC}$ Analyses

The $\delta^{13}C_{DIC}$ (n = 279, 10 expeditions) samples were prepared and analyzed at MARUM-Bremen, WHOI-Massachusetts, and the Museum für Naturkunde-Berlin laboratories (see Tables 1 and S4). Preparation involved the injection of an aliquot of 2 mL of seawater through a septum into a vial with 1 mL concentrated phosphoric acid flushed with pure helium. The resulting full batch of samples was kept at room temperature for at least 6 hr to enable full reaction between the DIC and the acid to produce CO_2. $\delta^{13}C_{DIC}$ were determined using a Thermo Fisher Gas Bench II coupled to a Thermo Finnigan MAT 252 mass spectrometer and Thermo Fisher Scientific Delta V. The standard deviation for all laboratories was based on routine measurements of the internal standard Ground Solnhofen Limestone-SHK Br2008 ($\delta^{13}C$: −0.96‰) and was better than 0.1‰. Working standards were calibrated against NBS 19 ($\delta^{13}C$: +1.95‰; Brand et al., 2014), NBS 18 ($\delta^{13}C$: −5.01 ± 0.03; Brand et al., 2014). All results were then corrected to VPDB. To complement our new data, we include in the database the published $\delta^{13}C_{DIC}$ values for the SEP (n = 1552, 4 expeditions, see Table S4). This data was prepared following the WOCE protocols and the data are stored in the GLODAP database https://www.glodap.info/.

The burning of fossil fuels since the Industrial Revolution has led to the long-term depletion of $\delta^{13}CO_2$ in the atmosphere, which in turn is affecting seawater $\delta^{13}C_{DIC}$ values (e.g., ref. Suess Effect; Keeling, 1979; Suess, 1955). The maximum Suess effect in the SEP is found in surface waters reaching between −0.6‰ and −0.4‰ at 100 m, −0.4‰ and −0.2‰ at 200 m, −0.2‰ and −0.05‰ at 300–400 m. Below 800 m no depleted $\delta^{13}CO_2$ has been registered so far (Eide et al., 2017). The maximum Suess effect in SEP waters has been computed by global compilations which only consider the regional P06 WOCE line expeditions from 1992, 2003, and 2010 (316N138-3/49NZ20030303/318M20100105). Due to the low amount of temporal and spatial $\delta^{13}C_{DIC}$ data for the SEP used for Suess effect estimations, in this study the corrections are not applied. We provide raw data from 1992 to 2018 which offer an accurate distribution of the tracers that can be used as a modern analogue for regional paleoceanographic reconstructions.

3.3.3. $\delta^{13}C$ From Air-Sea Exchange ($\delta^{13}C_{air\text{-}sea}$)

For the samples with $\delta^{13}C_{DIC}$ and phosphate measurements, the $\delta^{13}C_{air\text{-}sea}$ exchange values were calculated (Table 3) based in the equation proposed by Broecker and Maier-Reimer (1992) and reviewed by Lynch-Stieglitz et al. (1995). $\delta^{13}C_{air\text{-}sea}$ explains how much a water mass can be affected by the fractionation of carbon isotopes in surface waters due the exchange of CO_2 between the atmosphere and the surface ocean. To calculate $\delta^{13}C_{air\text{-}sea}$ the $\delta^{13}C_{DIC}$ values are corrected using the Redfield relationship from the deep Pacific/Indian Ocean:

$$\delta^{13}C_{air\text{-}sea} = \delta^{13}C_{DIC} + 1.11 \times PO_4 - 2.7$$

3.3.4. Stable Isotope End-Member Calculations

Once the composition of the water mixture at each sampled point was calculated using the EOMP, the source water types (i.e., end-members) of $\delta^{18}O$, δD, and $\delta^{13}C_{DIC}$ values for each water mass were computed by resolving (through least-squares) in a system of linear equations (one per sampled point with EOMP solution) with the unknowns being now the isotopic end-members and the coefficients being the previously computed water mass contribution in each sampled point. The maximum error of the EOMP analysis is

4%. Because $\delta^{13}C_{DIC}$ is considered a non-conservative tracer, the system of equations includes the remineralization and denitrification as coefficients previously computed by Llanillo et al. (2013).

3.4. Water Mass Temperature, Salinity, Nutrients, and Stable Isotope Statistical Analyses

The values considered for statistical analyses (mean and standard deviation, $\mu \pm 1\sigma$) only reflect samples marked by a dominant water mass (>50% contribution, calculated using EOMP analysis) and which are from below the mixed layer (>55 m).

Because of this criteria no statistical analyses were carried out for $\delta^{18}O$ and δD of the oceanic section. Temperature, salinity, oxygen, nutrients (phosphate, nitrate, nitrite, and silicate), and $\delta^{13}C_{DIC}$ data did meet this criteria for the oceanic and coastal sections. Table 3 and Figures S1–S9, summarized the $\mu \pm 1\sigma$ results for all hydrological parameters classified by water mass and region.

To assess whether it is possible to use the $\delta^{18}O$, δD, and $\delta^{13}C_{DIC}$ to trace water masses through paleoceanographic reconstructions, we statistically differentiate the signatures of the main water masses in the SEP using histograms (Figures S8 and S9) and non-parametric Mann-Whitney pairwise testing. These analyses clearly distinguish the degree of overlap between tracer values of the individual water mass.

3.5. Data Visualization and Processing

For data visualization we use Ocean Data View 5.2.1 (Schlitzer, 2021; https://odv.awi.de/). The original data for the meridional section plots were gridded using interpolated variational analysis (DIVA, https://github.com/gher-ulg/DIVA) and weighted-average interpolation. The degree of gridding was maximum 35 in the coordinate axis (X) and 45 in the axis (Y). For the EOMP analysis, a MATLAB code was developed by Llanillo et al. (2012, 2013).

A Python code was developed for statistical analyses and data manipulation using elements of the free and open-source library SciPy for scientific and technical computing https://www.scipy.org/. For further information see https://github.com/Paleobiogeochemistry.

4. Results and Discussion

We present the first isotope characterization of the main water masses of the SEP in order to validate $\delta^{18}O$, δD, and $\delta^{13}C_{DIC}$ as past water mass tracers (i.e., proxies). Our work provides unique information that compiles a long-term data set of 20 yr, serving as the first isotopical geochemical baseline for future initiatives aimed at testing detailed paleoceanographic dynamics in the SEP.

4.1. Distribution and Mixing of Southeast Pacific Water Masses

Our EOMP analysis reveals that north of ~30°S STW dominates in the oceanic section in the upper 200 m, contributing >60% to the water mixture (Figure 3a). In the coastal section, STW contributes only 40%–50% of the water mass (Figure 3b) due to horizontal mixing with SAAW and vertical mixing (upwelling) with ESSW (Figures 3b and 3f), confirming results by Silva et al. (2009).

South of ~25°S, the SAAW contributes between 60% and 90% to the water mixture in the upper 300 m of the oceanic section and it subducts below the STW (Figure 3c). After the subduction, when the SAAW has become the ESPIW, its core (>50%, at ~200 m) can be traced until 20°S. Luyten et al. (1983), Schneider et al., (2003) and Hernández-Vaca et al. (2017) propose that SAAW is subducted into the ocean interior along the Subtropical Front due to wind-induced Ekman pumping. In the coastal section, SAAW dominates as a surface water mass as far north as ~30°S, without being subducted beneath the STW. We hypothesize that three processes prevent intense downwelling of the SAAW near the coast (a) riverine freshwater input along the coastal section, (b) coastal upwelling, and (c) the position further north of the Subtropical Front in the Chilean coast.

In the subsurface below STW and SAAW, ESSW can be found in the northern part of the whole SEP, cradling above and alongside AAIW between 100 and 700 m. Here ESSW makes up 50%–70% of the water mixture with its core centered at 500 m. The ESSW flows southward and is mixing with SAAW (above) and AAIW (below).

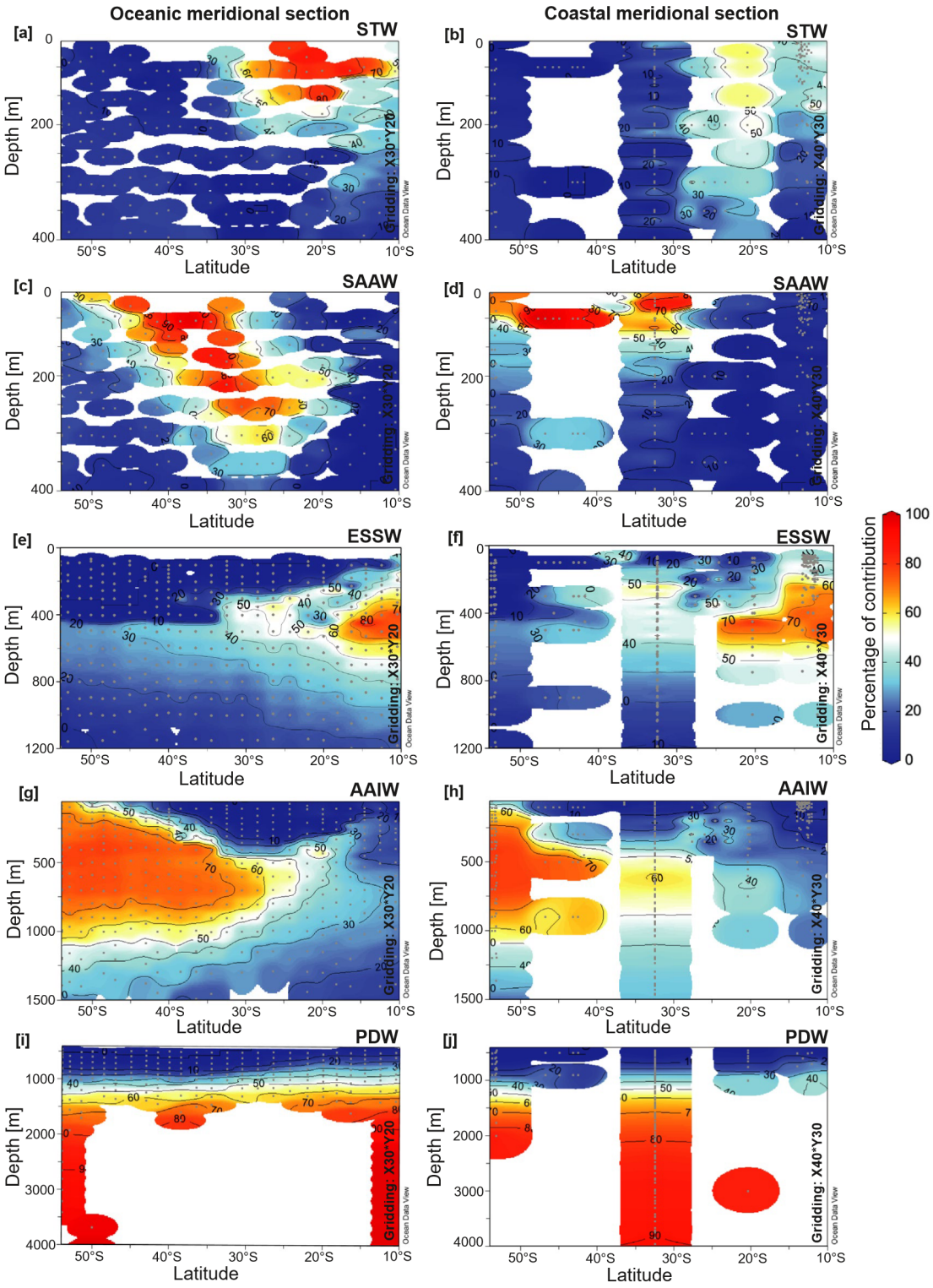

Figure 3. Relative water mass contribution from the water mixture in percentage (%) presented along the oceanic and coastal hydrological sections. Results were obtained using the extended optimum multiparameter (EOMP) analysis with the source water mass characteristics given in Table 3. The representation of the percentage distribution for each water mass is from top to bottom as STW (Subtropical Surface Water; (a) Oceanic section, (b) Coastal section), SAAW (Subantarctic Surface Water; (c) Oceanic section, (d) Coastal section), ESSW (Equatorial Subsurface Water; (e) Oceanic section, (f) Coastal section), AAIW (Antarctic Intermediate Water; (g) Oceanic section, (h) Coastal section), and PDW (Pacific Deep Water; (i) Oceanic section, (j) Coastal section). Each site is represented by gray dots. The degree of gridding is indicated in the sections. Samples from the mixed layer (uppermost 55 m) were not included in the analysis. Grey dots show sample sites.

While this mixing is limited to ~20° to 30°S in the oceanic section (Figures 3e–3f), ESSW is prominent (30% and 50%) in the coastal section as far south as 40°S (Figures 3f and S3 at 50 m) with an upward expansion to 100 m water depth.

At the coastal section off Peru and northern Chile upwelling brings the ESSW closer to the surface. It also reaches a more southern position due to hydrostatic equilibrium where low ESPIW-SAAW contributions to depths >100 m allow ESSW to advance further south, transported by the PCUC along the continental slope until it is mixing with the AAIW and SAAW. Silva et al. (2009) found a much higher maximum contribution of >90% of the ESSW between 30° and 10°S between 100 and 500 m water depth in the oceanic section.

Beneath the SAAW and ESSW (54°–25°S), the northward flowing AAIW contributes between 70% and 50% to the water mixture down to depths of 1,200 m, both in the oceanic and coastal sections. In the south, the core of the AAIW is centered at ~600 m with a water column range between ~200 and ~800 m. Furthermore north, AAIW deepens to 400–800 m in the coastal section, whereas in the oceanic section it remains at a similar depth as in the south of the study region (Figures 3g and 3h). AAIW still contributes >50% at 20°S (oceanic section) and 25°S (coastal section), respectively, and becomes less important (<30%) between 20° and 15°S (oceanic and coastal sections; Figures 3g and 3h).

The water mass contribution results show that there are differences between the coastal and oceanic section above 1,000 m water depth (Figure 3). In the coastal section the STW has less predominance and mixes with the upper part of the ESSW. We observe that the ESSW can extends to southern latitudes than in the oceanic section. As well, we find that between the ESSW and the upper part of the AAIW is defined a large mixing zone that is not observed in the oceanic sections.

Toward deeper levels in the water column between 1,000 and 4,000 m, the PDW contributes progressively from 40% to 90% to the water mixture (Figures 3i and 3j). An upper (1,000–1,500 m) and a lower PDW (>1,500 m) can be separated by density; the upper horizon actively mixes with AAIW and ESSW whereas lower PDW is much purer. Our limited data suggests that there are no differences in PDW contribution offshore and onshore. Insufficient data prevents us from considering CDW in the extended EOMP analysis.

4.2. Water Mass Characterization for the Southeast Pacific Using Stable Isotopes of Oxygen, Hydrogen, and Carbon

4.2.1. Conservative Water Mass Tracers: Oxygen and Hydrogen Isotopes

The characterization of SEP water masses by $\delta^{18}O$ and δD is limited to the coastal section due to the scarcity of data in the oceanic section (Figures 4c–4f). For PDW it was not possible to calculate the mean and standard deviation ($\mu \pm 1\sigma$) due the limited data availability.

The STW, SAAW, ESSW and AAIW maintain their source region $\delta^{18}O$ and δD (Figures 1d; Tables 2 and 3). The relatively heavy STW isotopic composition (Figures 5 and S8; Table 2) suggests that this water mass originates from a region with high evaporation rates (Conroy et al., 2017). This is consistent with earlier work showing that the STW is formed in the northern part of the high-pressure Subtropical Pacific Gyre region (Stramma et al., 1995; Wyrtki, 1973). Because of the hyperarid climate in southern Peru/northern Chile, the limited discharge of freshwater indeed does not affect the $\delta^{18}O$ and δD signature of the broader STW. However, the isotopic values combined with temperature and salinity, provide evidence that STW is mixed with upwelled ESSW between 10° and 32°S (Figures 4b, 4d, 5g, and 5h).

The SAAW has comparably low $\delta^{18}O$ and δD values (Figure 4b, 4d, 5g, and 5h; Table 2). This is related to high rates of precipitation over the Subantarctic Zone (Bass et al., 2014) and the input and subsequent mixing of freshwater coming from discharge of meltwater directly from the humid southern Patagonian glaciers. Temperature/salinity diagrams of the oceanic (Figure 5a) and coastal (Figures 5g and 5h) sections, clearly reveal that coastal SAAW is fresher than its oceanic counterpart, indicating the dominance of the SSAAW (Davila et al., 2002; Llanillo et al., 2012; Rojas & Silva, 1996; Silva et al., 2009; Silva & Neshyba, 1979/1980).

Similar to STW, the ESSW is marked by relatively high isotopic values, indicating that it is formed in the Equatorial Pacific region where evaporation exceeds precipitation. Once ESSW mixes with AAIW and SAAW off central-southern Chile, its values become modified (Figure 4b, 4d, 5g, and 5h; Table 2).

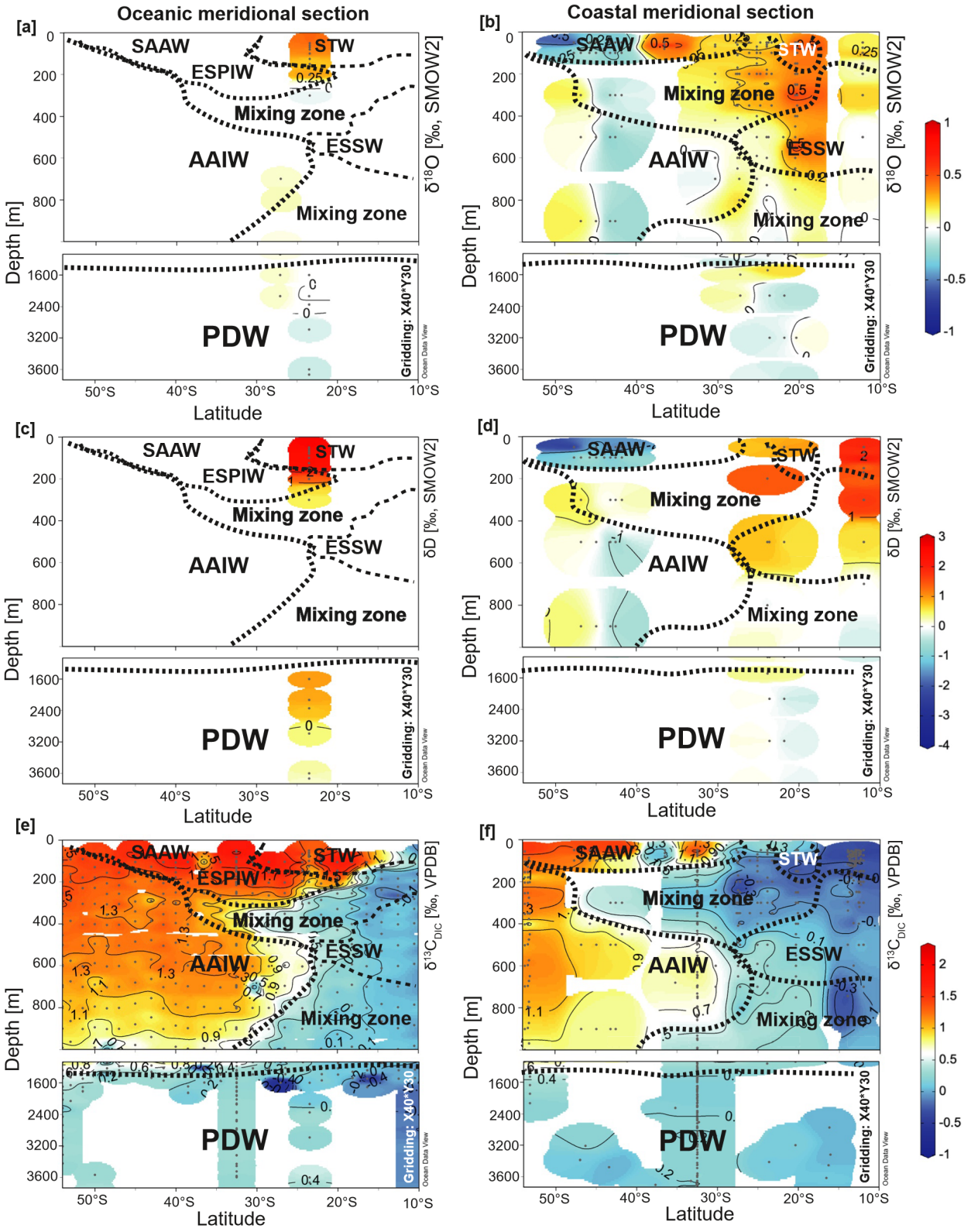

Figure 4. $\delta^{18}O$ (a and b), δD (c and d), and $\delta^{13}C_{DIC}$ (e and f) oceanic-coastal meridional sections in the Southeast Pacific. Main water masses can be seen in all the hydrological sections: STW (Subtropical Surface Water), SAAW (Subantarctic Surface Water), ESPIW (Eastern South Pacific Intermediate Water), ESSW (Equatorial Subsurface Water), AAIW (Antarctic Intermediate Water), and PDW (Pacific Deep Water). Small gray dots represent the sampling site. The degree of gridding is indicated in the sections. Dashed lines represent the isoline of 50% of the contribution of the water mass to the water mixture. Grey dots show sample sites.

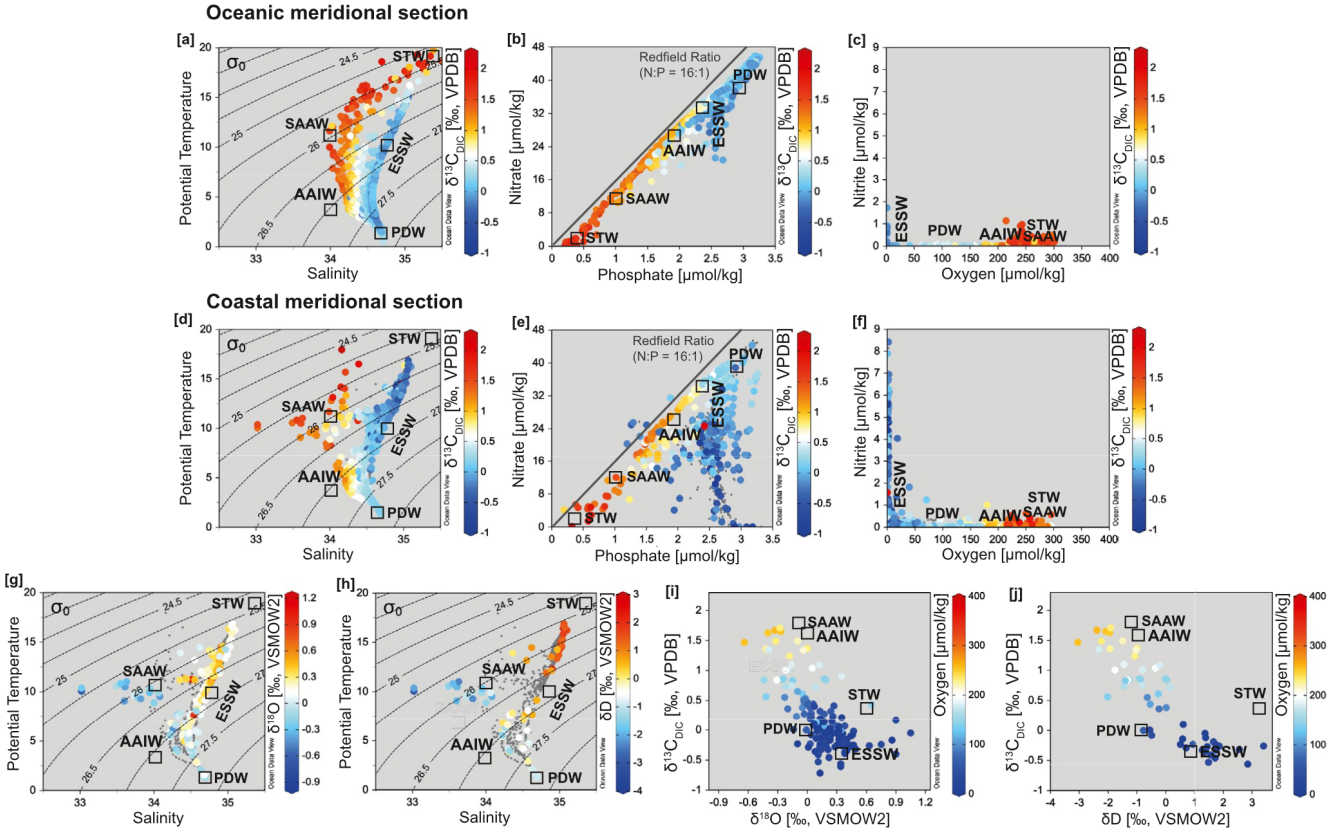

Figure 5. (a, d, g, and h) Potential temperature-salinity with density isopycnals. (b and e) Nitrate-Phosphate diagram, with Redfield ratio shown by a gray line. (c and f) Nitrite-Oxygen diagrams from the oceanic and coastal sections. (i and j) $\delta^{13}C_{DIC}$-$\delta^{18}O$ diagram. The figures are color-coded from (a) to (f) by $\delta^{13}C_{DIC}$ in (g) by $\delta^{18}O$ in (h) and by δD in (i and j) by oxygen concentrations. Water mass end-members characteristics are shown in black squares: STW (Subtropical Surface Water), SAAW (Subantarctic Surface Water), ESSW (Equatorial Subsurface Water), AAIW (Antarctic Intermediate Water), and PDW (Pacific Deep Water). Grey dots show sample sites.

The AAIW, as the SAAW, is formed in the southern section of the SEP (McCartney, 1977) and travels North toward the tropical east Pacific (Llanillo et al., 2018; McCartney, 1977). Its $\delta^{18}O$ value (Table 2) is similar to those reported previously for surface waters at the Subantarctic front (Bass et al., 2014; $\delta^{18}O$: −0.3‰ and δD: 0‰) implying that AAIW is also influenced by high oceanic precipitation. Slightly depleted δD values of AAIW could also result from the contribution of melting ice from the Patagonian Fjords.

Because there were only a few data points for PDW in the SEP we were not able to calculate mean and standard deviations ($\mu \pm 1\sigma$). Hence, these data should be taken with caution.

4.2.2. $\delta^{18}O$-Salinity and δD-Salinity Relationships in the Southeast Pacific

In the modern regional ocean, $\delta^{18}O$-salinity ($\delta^{18}O$-S) and δD-salinity (δD-S) relationships are used for understanding the ocean and atmosphere forcings that influence these, to enable potential reconstructions of past regional hydrographies (Benway & Mix, 2004; Bigg & Rohling, 2000; Conroy et al., 2017; LeGrande & Schmidt, 2006; Schmidt, 1998, 1999). LeGrande and Schmidt (2006) and Schmidt (2009) classified $\delta^{18}O$-salinity slopes and intercepts from surface waters from several regions worldwide. These authors concluded that steep slopes (around 0.5‰/sal) and low intercepts (around −15‰ and −17‰) characterize mid- and high-latitudes, where the $\delta^{18}O$ end-member of freshwater is controlled by local precipitation. In tropical regions, the $\delta^{18}O$ end-member is primarily controlled by evaporation. Therefore, the $\delta^{18}O$ signature in the lower latitudes is isotopically heavier due to the effect of evaporative fractionation. Slopes and intercepts for the respective $\delta^{18}O$-S relationship tend to be flat (0.1‰/sal–0.3‰/sal) and higher (from about −8‰ to −10‰).

There are no published δD-S relationships for the Pacific Ocean and our δD data set is small, therefore the main discussion is mostly based on the relationship between $\delta^{18}O$ and salinity. We are aware that our $\delta^{18}O$-S and δD-S

Table 4
$\delta^{18}O$-Salinity, δD-Salinity Relationships Results (Slopes, Intercepts, r^2, and p-Value) Determined for the Main Water Masses at the Southeast Pacific Compared With Published Data

Region or Water Mass	Year of sampling	Data points		Slope		Intercept		r^2		p-Value	
		$\delta^{18}O$	δD	$\delta^{18}O$	δD	$\delta^{18}O$	δD	$\delta^{18}O$	δD	$\delta^{18}O$	δD
This study											
SAAW	2010–2018	8	7	**0.81**	1.04	**−27.54**	−36.49	**0.57**	0.15	**0.03**	0.39
ESSW	2010–2018	22	9	−0.08	**4.12**	2.97	**−142.43**	0.00	**0.55**	0.83	**0.02**
Published data											
South Pacific (Schmidt, 1999)				0.63		−21.5		**0.78**			
Equatorial east Pacific (Schmidt, 1999)				0.10		−3.3		0.35			
Northeast Pacific (Schmidt, 1999)				0.37		−12.9		**0.96**			
GISS Central Tropical Pacific (0–75 m; Conroy et al., 2014)				0.23		−7.82		**0.88**			
GISS Central Tropical Pacific (80–500 m; Conroy et al., 2014)				0.35		−11.83		**0.83**			
Central Tropical Pacific Line Island Ridge (0–75 m; Conroy et al., 2014)				0.31		−10.38		**0.91**			
Central Tropical Pacific Line Island Ridge (80–500 m; Conroy et al., 2014)				0.42		−14.38		**0.94**			
Western Central Pacific Kiritimati (0–1 m; Conroy et al., 2017)				0.17		−5.5		0.37			
Western Central Pacific Manus, Papua (0–1 m; Conroy et al., 2017)				0.20		−6.6		**0.93**			
East Equatorial Pacific Galapagos (0–1 m; Conroy et al., 2017)				0.08		−2.4		**0.85**			
Panama Bight (0–40 m; Benway & Mix, 2004)				0.25 and 0.14		−8.52 and −4.80		**0.98 and 0.84**			
Panama Bight (41–400 m; Benway & Mix, 2004)				0.47		−16.15		**0.55**			
Panama Bight (>400 m; Benway & Mix, 2004)				−1.89		65.42		**0.95**			
Deep Pacific/Indian (LeGrande & Schmidt, 2006)				−0.41		14.25		0.03			

Note. Regressions were performed for water masses with more than five data points. Significant relationships ($p \leq 0.05$) are indicated by bold font.

results rely on a small region and they are analyzed by each water mass. Further studies will be required for evaluating if the relationship between stable isotope and salinity could be extended for large areas as well as for understanding water mass processes.

For some SEP water masses the $\delta^{18}O$ values overlaps (Tables 3 and S5), which is clearly seen in the $\delta^{18}O$-S relationships (Figure S13 in Supporting Information S1). In contrast, the δD-S relationship shows no overlapping in the δD values. Therefore, our results suggest that δD could be a promising tracer for water masses in the region. SAAW and ESSW are unique in that they exhibit statistically significant ($p < 0.05$) $\delta^{18}O$-S and δD-S relationships. Both water masses feature a steep slope and low intercept (Figure S13 in Supporting Information S1; Table 4). Our results confirm previous work by LeGrande and Schmidt (2006) suggesting that SAAW is formed in the high southern latitudes (Table 4) and indicate the absence of sea-ice formation in the coastal region of the SEP (Figure S13). Indeed, the strong winds and low pressure system in the Subantarctic Zone bringing high rates of precipitation adding to the input of meltwater from Southern Patagonia are the principal mechanisms explaining the $\delta^{18}O$-S and δD-S relationship for the SAAW.

The δD-S relationship for the ESSW follows the opposite trend expected for tropical regions (i.e., flat slopes and high intercepts). It is likely that the ESSW δD-S relationship is affected by vertical mixing (e.g., Conroy et al., 2014), causing the loss of its expected δD-S and $\delta^{18}O$-S relationships typical for a tropical water mass (Figure S13; Table 4).

4.2.3. Non Conservative Water Mass Tracers and the Carbon Isotopic Composition ($\delta^{13}C_{DIC}$) of the Main SEP Water Masses

The spatial extent of available and new $\delta^{13}C_{DIC}$ data in the SEP allows us to expand the discussion of its $\delta^{13}C_{DIC}$ distribution, especially in the coastal section (Figures 4e–4f). SAAW, ESSW, AAIW, and PDW appear to be semi-conservative, maintaining $\delta^{13}C_{DIC}$ signatures from their source region (Figure 1d; Tables 2 and 3).

For STW, the mean $\delta^{13}C_{DIC}$ values in the coastal section are depleted compared to the oceanic section and the oceanic end-member (Figures S9 and S14; Tables 2 and 3). Nutrient contents (silicate, phosphate, and nitrate; Figures 2 and S3–S7; Table 3) and $\delta^{13}C_{air\text{-}sea}$ values are high in the coastal section compared with the oceanic sections (Figures S15 and S16; Table 3). Nitrate production is obvious in the STW in the coastal section (Figure 5f; Table 3) confirming previous studies that report that anaerobic anammox and/or denitrification processes are important in the upper part of the OMZ off Peru/Chile (Codispoti & Christensen, 1985; Hamersley et al., 2007; Llanillo et al., 2013; Thamdrup et al., 2006). We propose that depleted $\delta^{13}C_{DIC}$ and high $\delta^{13}C_{air\text{-}sea}$ values in the coastal section are related to vertical mixing of STW with $\delta^{13}C_{DIC}$-depleted ESSW. The phosphate and nitrate concentration in the STW follow Redfield ratios (Figures 5b and 5e).

In contrast to the STW, SAAW exhibits high values of $\delta^{13}C_{DIC}$ with relative low $\delta^{13}C_{air\text{-}sea}$ in the coastal and oceanic sections (Figures S9 and S14–S16; Table 3) with high oxygen and low nutrient contents (silicate, phosphate, nitrate, and nitrite; Figures 2 and S3–S7; Table 3). The high $\delta^{13}C_{DIC}$ and oxygen content and low $\delta^{13}C_{air\text{-}sea}$ and nutrients values of SAAW reflect the high ventilation in the formation zone of the water mass. The silicate and phosphate content is slightly higher in the coastal than in the oceanic section (Figure 2; Table 3), reflecting additional nutrient input by river/fjords runoff (between 54° and 36°S) and upwelling of ESSW (between 38° and 32°S; Vargas et al., 2016 and 2018). A lack of nitrite confirms that redox processes within the SAAW are weaker compared with STW. We suggest that the slight excess in phosphate in the coastal region is sourced from the southern upwelling cells that exhibit relatively low values of $\delta^{13}C_{DIC}$ (Figure S12). In both oceanic and coastal sections, the phosphate and nitrate values of the SAAW follow the Redfield ratio (Figures 5b and 5e).

The subsurface ESSW show low $\delta^{13}C_{DIC}$ and oxygen values, with high nutrient contents (silicate, phosphate, nitrate, and nitrite; Figures 2, S3–S7, S9, and S14; Table 3) and $\delta^{13}C_{air\text{-}sea}$ in the coastal and oceanic sections (Figure S15; Table 3). These results may be explained by the accumulation of respired ^{12}C during the passage of the ESSW along the highly productive upwelling systems off western South America and in situ intense redox processes in the coastal section (Chavez & Messié, 2009; Daneri et al., 2000; Montero et al., 2007; Vergara et al., 2017). Close to the coast methanogenesis within suspended particles has been observed in the pycno/oxyclines (Holmes et al., 2000; Naqvi et al., 2010; Sansone et al., 2001; Troncoso et al., 2018), resulting in the accumulation of methane depleted $\delta^{13}C$ (Tenorio, 2021). This process may also be responsible for some of the highly depleted $\delta^{13}C_{DIC}$ values observed in ESSW. In the coastal section the phosphate and nitrate concentration in the ESSW diverge from Redfield ratios, in contrast to the oceanic section (Figures 5b and 5e), a feature previously reported to be typical for the SEP-OMZ (Llanillo et al., 2012; Silva et al., 2009). High nitrite contents are found in the ESSW reaching up to 7 μmol kg^{-1} in the coastal section (Figures 5f and S6; Table 3). The presence of nitrite is best explained by the reduction of nitrate to nitrite via denitrification within the core of the OMZ (e.g., Farías et al., 2007; Graco et al., 2007; Llanillo et al., 2013; Silva et al., 2009).

The AAIW has high and similar $\delta^{13}C_{DIC}$ values along the coastal and oceanic sections. $\delta^{13}C_{air\text{-}sea}$ values are near to zero, similar to that of SAAW (Figures S14 and S15; Table 3). The AAIW exhibits relatively high values of oxygen and low nutrient content (as silicate, phosphate, nitrate, and nitrite; Figures 2 and S3–S7; Table 3). The phosphate and nitrate concentration in the AAIW is roughly aligned with redfield ratios in the oceanic and coastal section (Figures 5b and 5e) and a negligible nitrite production (<0.4 μmol kg^{-1}) is found (Figure 5f; Table 3). The similar $\delta^{13}C_{air\text{-}sea}$ values of AAIW and SAAW confirm that AAIW is well ventilated with a relatively young age, reinforcing previous work indicating that the SEP is the main formation region for AAIW (e.g., Bostock et al., 2010, 2013; Piola & Gordon, 1989). On its way north, the AAIW vanishes around 32°–30°S in the coastal section and at 24°S in the oceanic section. There is a progressive northward depletion in the AAIW $\delta^{13}C_{DIC}$ values

from +0.9‰ to +0.4‰ between 32° and 24°S (Martínez-Méndez et al., 2013a) due to mixing with ESSW/PDW in the lower part of the SEP-OMZ (Figure 4f).

The PDW has relatively low $\delta^{13}C_{DIC}$ values (Figures 4 and S14; Table 3) in the coastal and oceanic section. Oxygen levels are low and nutrient contents (as silicate, phosphate, and nitrate) are high (Figure 2; Table 3). The phosphate and nitrate concentrations in the PDW are aligned with the Redfield ratio in the oceanic and coastal sections (Figures 5b and 5e). Thus, the PDW is marked by a high content of respired ^{12}C (inferred from the high nutrient concentration) and is a poorly ventilated water mass. We do not include in the discussion the computed values for $\delta^{13}C_{air\text{-}sea}$ (Figures S15 and S16; Table 3) for the PDW. As explained above, it is a mixture of water masses with several sources and does not have any active exchange with the atmosphere.

In the coastal section the PDW/ESSW/AAIW mixing zone (Figure 4) exhibits relatively lower $\delta^{13}C_{DIC}$ values than in the oceanic section. This feature is not traceable with temperature, salinity, oxygen and phosphate, suggesting that depleted $\delta^{13}C_{DIC}$ from the OMZ/ESSW can reach deep waters and influence the distribution of this tracer in the coastal section (Silva et al., 2009; Vargas et al., 2021).

Between 200 and 1,800 m within ESPIW, AAIW, and PDW there are localized spots in the oceanic section that display very low $\delta^{13}C_{DIC}$ values (Figure 4), which may be caused by mesoscale eddies (Zhang et al., 2014). It has been observed that surface-to-deep eddies originating in the coastal section of the SEP can be advected far offshore into the oceanic section, contributing to long-distance biogeochemical transport affecting the characteristics of the water column (Czeschel et al., 2018). We suggest that such eddies possibly originate in the coastal zone transferring ESSW characteristics to intermediate and deep waters in the oceanic section of the study area.

In summary we find major differences in $\delta^{13}C_{DIC}$, nutrients, and oxygen content between the coastal and the oceanic section. We propose (a) the absence of the ESPIW in the coastal zone allowing the low oxygen, high nutrients, $\delta^{13}C_{DIC}$ depleted waters originating from the ESSW to extend much further south up to ~48°S there, while such waters are restricted to <30°S in the oceanic section, (b) the very different oxygen, nutrients, and $\delta^{13}C_{DIC}$ signatures of the STW along the two sections causing a significant depletion of $\delta^{13}C_{DIC}$ in the coastal section, and (c) the enhanced mixing of the upper-AAIW with ESSW resulting in lower average oxygen and $\delta^{13}C_{DIC}$ values in the coastal AAIW. These differences, especially in the upper ~1,000 m of the water column highlight the value of such coastal data for paleoceanographic reconstructions which are often based on sedimentary records from the continental margin.

4.2.4. Paleoceanographic Implications

Within the limitations described above**,** our new $\delta^{18}O$, δD, $\delta^{13}C_{DIC}$, temperature, salinity, oxygen, and nutrient data combined with the percentage contribution per water mass (Figures 2–5 and S1–S9; Tables 2 and 3) can be used to differentiate modern water mass geometry (i.e., water mass distribution) in the SEP. This characterization improves our understanding of chemical processes within water masses, and can contribute to regional proxy calibrations.

Statistical analyses (i.e., Mann-Whitney tests) allow us to differentiate oxygen, hydrogen, and carbon stable isotopic values of the main water masses (Tables S5–S7). This considers mean isotopic values of each water mass and compares them to establish which water masses are isotopically correlated. We are aware that data for δD are still limited for the SEP, and patterns described here should be confirmed as further stable hydrogen isotope data become available. This is especially true for the PDW, which was excluded from Mann-Whitney analyses due to insufficient data. Thus, based on $\delta^{18}O$ and δD, SAAW/STW, SAAW/ESSW, and ESSW/AAIW can be differentiated, but not STW/ESSW, SAAW/AAIW, ESSW/PDW, and AAIW/PDW. While $\delta^{13}C_{DIC}$ can be used to differentiate between STW/ESSW (oceanic section), SAAW/ESSW, ESSW/AAIW, and AAIW/PDW, but not SAAW/STW and STW/ESSW (coastal section).

For reconstructions of past seawater salinities and temperatures, one important tracer is the oxygen isotopic composition of calcifiers, such as foraminifera. Hebbeln et al. (2000) and Mohtadi et al. (2005) studied the $\delta^{18}O_{calcite}$ in core-top planktonic foraminifera from a North-South latitudinal transect across the SEP, showing that foraminifera grown in the STW are relatively depleted compared to the ones from the SAAW. This suggests that planktonic foraminifera $\delta^{18}O_{calcite}$ is a possible route to study changes in the distribution of these surface waters in the past. Caniupán et al. (2011), Nürnberg et al. (2015), and Haddam et al. (2018) have subsequently used

planktonic foraminifera $\delta^{18}O_{calcite}$ to study changes in the spatial variations of oceanic fronts and surface water masses in the SEP.

It is important to note that the $\delta^{18}O_{calcite}$ composition of foraminifera is influenced by $\delta^{18}O_{sw}$ (closely coupled to salinity), temperature, vital and calcification effects, and ice volume (Bemis et al., 1998; Epstein et al., 1953; Lynch-Stieglitz et al., 1999; Marchitto et al., 2014; O'Neil et al., 1969; Shackleton, 1967; Urey, 1947). Temperature exerts a strong control on $\delta^{18}O_{calcite}$. Past temperature variations are commonly resolved by proxies, such as Mg/Ca ratios, or alkenones. $\delta^{18}O_{calcite}$ has uncertainties in the order of >0.2‰ that represent 1°C (Pearson, 2012). Over glacial-interglacial timescales global $\delta^{18}O_{sw}$ varies by ~1.0‰–1.2‰ (Fairbanks, 1989). Together, temperature and ice-volume related uncertainties result in a ±0.4‰ uncertainty in reconstructions of past $\delta^{18}O_{sw}$ values. This is very close to the range of SEP $\delta^{18}O_{sw}$ end-member values observed today. Within the SEP, the highest difference in $\delta^{18}O_{sw}$ end-member values (0.72‰) is observed between STW and SAAW (e.g., STW and ESSW = 0.29; SAAW and ESSW = 0.43; ESSW and AAIW = 0.31, ESSW and PDW = 0.21; AAIW and PDW = 0.01). Unless these uncertainties can be reduced, and/or past end-members become statistically different, it is unlikely that reconstructions of past $\delta^{18}O_{sw}$ values will provide statistically meaningful information about water mass distributions within the SEP.

The lack of local equations for describing the $\delta^{18}O$-S relationship leads to additional uncertainties in paleosalinity reconstructions based on $\delta^{18}O_{sw}$ (Schmidt, 1999). In this regard, our results suggest that salinity inferences could be indeed implemented in the SEP, especially for SAAW and ESSW (Figure S13; Table 4), considering $\delta^{18}O$-S and δD-S relationships documented here. Nevertheless, these regional paleosalinity reconstructions should rely on the assumption that such relationships remained unchanged over time. The use of the δD-S relationship either for salinity reconstructions or differentiation of water masses is a striking result, with deep implications for paleoceanographic reconstructions. Still, its potential must be explicitly revised as more stable hydrogen isotopic characterization of water masses in the SEP are conducted and validated.

The carbon isotopic composition of foraminifera ($\delta^{13}C_{calcite}$) from the fossil record is also often used for water mass reconstructions. The $\delta^{13}C_{calcite}$ in foraminifera is influenced by the ambient $\delta^{13}C_{DIC}$ and vital effects such as metabolic precipitation of calcium carbonate, respiration and symbiont photosynthesis (e.g., Ishimura et al., 2012; Mackensen et al., 1993; McCorkle & Keigwin, 1994; Spero, 1992; Spero et al., 2003). Some epifaunal benthic (living on top of sediments) have $\delta^{13}C_{calcite}$ that is similar (1–1 relationship) to bottom water $\delta^{13}C_{DIC}$ and can be used for reconstruct changes in ventilation and distribution of their habitat water masses (e.g., Schmittner et al., 2017).

Martínez-Méndez et al. (2013a) and Haddam et al., (2020) used $\delta^{13}C_{calcite}$ in epifaunal foraminifera in sediment records from 27°S (970 kys) and 40°–50°S (23 kys), respectively. Comparing epifaunal $\delta^{13}C_{calcite}$ with $\delta^{13}C_{DIC}$ values in situ (Martínez-Méndez et al., 2013a) and extrapolated from the oceanic region (Haddam et al., 2020) they reconstructed AAIW and PDW/CDW variability through time. The reconstructed $\delta^{13}C_{calcite}$ values in the sediment records are in a similar range as modern $\delta^{13}C_{DIC}$ values for AAIW and PDW.

Despite common strong vital effects, planktonic foraminifera $\delta^{13}C_{calcite}$ often indicate changes in surface to intermediate water masses geometry, ventilation, and productivity (e.g., Hebbeln et al., 2000; Mohtadi et al., 2008; Tapia et al., 2015, 2019). In the coastal section, the water masses show $\delta^{13}C_{DIC}$ end-member differences in a range of 2.29 and 0.52 (e.g., STW and SAAW = 1.39; STW and ESSW = 0.9; SAAW and ESSW = 2.29; ESSW and AAIW = 2, ESSW and PDW = 0.52; AAIW and PDW = 1.55). Thus, using epifaunal and planktonic foraminifera in the region could provide statistically meaningful information about changes in the characteristics of the water mass distributions within the coastal SEP.

$\delta^{13}C_{calcite}$ of planktonic foraminifera also may be used to reconstruct changes in surface waters within the SEP. Hebbeln et al. (2000) and Mohtadi et al. (2005) characterized the $\delta^{13}C_{calcite}$ of surface and subsurface planktonic foraminifera from core top samples recovered in a north-south transect in the coastal SEP. They found that surface planktonic foraminifera recorded low $\delta^{13}C_{calcite}$ beneath the STW compared to high $\delta^{13}C_{calcite}$ beneath the SAAW, corresponding to the regional productivity-upwelling patterns. These results are similar to $\delta^{13}C_{DIC}$ values of the surface waters indicating that planktonic foraminifera $\delta^{13}C$ in the region can be used as a proxy for surface water $\delta^{13}C_{DIC}$.

In terms of using $\delta^{18}O_{calcite}$, in combination with temperature reconstructions, to calculate $\delta^{18}O_{sw}$, to trace water masses it may be useful to compare this with $\delta^{13}C_{calcite}$, in a multi-proxy approach. Hebbeln et al. (2000) plotted for the first time $\delta^{18}O_{calcite}$ versus $\delta^{13}C_{calcite}$ in planktonic foraminifera for the SEP, showing a regional relationship that can be used for reconstructing the geometry of surface water masses. Our results show that $\delta^{18}O$ or δD and $\delta^{13}C_{DIC}$ relationships in sea water can be used as a modern analog for water mass geometry reconstructions (by time slices) in the region from surface to deep (Figures 5i and 5j).

Most paleoceanographic reconstructions for the SEP from the late Quaternary are based on sediment cores collected from the continental margin. During the last decades, these records were generally compared with open ocean data, because data from nearer to the coast was lacking (e.g., Castillo et al., 2017; De Pol-Holz et al., 2006, 2007; Haddam et al., 2018, 2020; Siani et al., 2013). Our new compilation of $\delta^{13}C_{DIC}$ data combined with temperature, salinity, oxygen, and nutrient data (Figures 2 and 4) reveal significant differences in the distribution of water masses in the upper ~1,000 m of the water column between the oceanic and the coastal sections. Our data furthermore expose a general absence of the ESPIW (subducted SAAW) in the coastal section (Figures 2–4). This puts some caveats on interpretations of previous studies (e.g., De Pol-Holz et al., 2006, 2007 and Castillo et al., 2017) that considered ESPIW as the main water mass that ventilates the upper part of the coastal ESSW/SEP-OMZ. Instead we argue that in the coastal section SAAW and AAIW might play a similar role as open ocean ESPIW, in ventilating the upper ESSW.

5. Conclusions

We present the first spatial characterization of $\delta^{18}O$, δD, and $\delta^{13}C_{DIC}$ along with temperature, salinity, oxygen, and nutrient contents of the main water masses in the SEP in an oceanic and a coastal section. Our analysis reproduces the well-known oceanic distribution of the main SEP water masses, originating in the equatorial, subtropical and subantarctic Pacific regions and it is the first one to include a highly resolved EOMP analysis of AAIW and PDW in the coastal SEP. However, our data also reveal that the water column structure in the coastal section clearly deviates from its oceanic counterpart, especially due to the absence of the ESPIW in the coastal section.

For past oceanographic reconstructions on marine sediment, we can use $\delta^{18}O$ and δD to differentiate between SAAW/STW, SAAW/ESSW, and ESSW/AAIW, but not between STW/ESSW, SAAW/AAIW, ESSW/PDW, and AAIW/PDW. $\delta^{18}O$-S and δD-S relationships are statistically significant for the SAAW and ESSW, suggesting that the SAAW have an origin in high-latitudes with strong influences of high precipitation and melted-ice from the Patagonian Ice Sheet. Our study confirms that ESSW follows an opposite trend expected for tropical regions, possibly due to advection and mixing processes with surface waters. $\delta^{13}C_{DIC}$ can be used as a proxy to differentiate between STW/ESSW (oceanic section), SAAW/ESSW, ESSW/AAIW, and AAIW/PDW, but not between SAAW/STW and STW/ESSW (coastal section). The $\delta^{13}C_{DIC}$, oxygen, and nutrients database for the oceanic section has a good spatial cover and can be compared with the new coastal data set, highlighting strong differences in water mass geometry above 1,000 m water depth in the SEP. In the coastal section, (a) the surface waters fill a smaller depth range, (b) the ESPIW (subducted SAAW) is absent allowing ESSW to spread much further south, (c) the STW $\delta^{13}C_{DIC}$ signature differs considerably from its oceanic counterpart, (d) the upper-AAIW with ESSW resulting in lower average oxygen and $\delta^{13}C_{DIC}$ values in the coastal AAIW, and (e) the PDW/ESSW/AAIW mixing zone shows lower $\delta^{13}C_{DIC}$ values than in the oceanic section. All these differences result in on average lower $\delta^{13}C_{DIC}$ values in the coastal section that partly deviate by >1‰ from the comparable depth/latitude setting in the oceanic section. These deviations clearly point out that it is necessary to compare paleoceanographic records recovered from intermediate waters along the western South American continental margin with present-day hydrological analogs from the coastal section.

The relationships of $\delta^{18}O$, δD, and $\delta^{13}C_{DIC}$ with each other and with other parameters like temperature and oxygen offer a multiproxy database that can be used as present-day hydrological analogs for reconstructions of past water mass distributions. In addition, using the relationship of planktonic and epifaunal benthic foraminifera $\delta^{18}O_{calcite}$ versus $\delta^{13}C_{calcite}$ in specific time slices may enable the characterization of past SEP water column geometries from surface to deep waters.

Data Availability Statement

All seawater hydrological and stable isotope data used here are provided in the supplementary materials and have been submitted to PANGAEA (https://www.pangaea.de/), GLODAP (https://www.glodap.info/) and NASA/GISS Global Seawater Oxygen Isotope Data Base (https://data.giss.nasa.gov/o18data/).

Acknowledgments
We thank the crews and scientific parties of research cruises R/V Sonne (SO102, SO245, SO211, and SO261), R/V Meteor (M93), R/V Roger Revelle RR9702A (GENE03RR), BIC José Olaya Balandra (Crio1812), R/V Cabo de Hornos (Cimar 21, LOWPHOX 1, Expedición TAITAO), and L/C Kay-Kay 2 (Station 18). We thank the invaluable help of Henning Kuhnert, Birgit Meyer-Schack and Wolfgang Bevern (Isotope Laboratory, MARUM), Martin Kölling (Sediment Geochemistry Laboratory, MARUM), Carol Arrowsmith (Isotope Laboratory BGS, UK), Josefa Verdugo (Biogeochemistry Laboratory, AWI), Alejandro Avila and Paola Cárdenas (Paleoceanography Laboratory, UdeC), Karen Sanzana (Isotope Biogeochemistry Laboratory, UdeC), Gerardo Garcia (IMO, UdeC), Frank Wenzhöfer and Timothy Ferdelman (AWI/Max-Planck-Institut für Marine Mikrobiologie, Bremen), Sara Nicolson and Alina Wiercorek (National University of Ireland Galway), Victor Aramayo (Meiobenthos Laboratory, IMARPE), Katy Cordova (Universidad Peruana Cayetano Heredia), Consuelo Martínez-Fontaine (Paleoclimat, Universities of Paris Sud and Paris-Saclay), Osvaldo Ulloa (Marine Microbiology Laboratory and IMO, Udec) and Michelle Ferrer (Universidad de Chile). We thanks to Kris Karnauskas (editor in Chief), Edith Judd (editorial office) and the Wiley Book production team from the JGR-Ocean. As well to the three anonymous reviewers for their constructive feedback on an earlier version of this manuscript. R/V Sonne cruises (SO102, SO211 ad SO245) were financed by the German Federal Ministry of Education and Research projects #03G0102A, #03G0211A and #03G0245A. SO261 cruise was funded by the HADES-ERC Advanced Grant ("Benthic diagenesis and microbiology of hadal trenches" Grant agreement No. 669947) awarded to R. N. Glud (SDU, Denmark). SO245 cruise recived contributions from the Max Planck Society (Germany), the German State of Lower Saxony, the National Environmental Research Council of Great Britain and the Science Foundation of Ireland. R/V Meteor cruise M93 was financed by the Sonderforschungsbereich 754 "Climate-Biogeochemistry Interactions in the Tropical Ocean" (www.sfb754.de), which is supported by the Deutsche Forschungsgemeinschaft. "Expedición TAITAO" was financed by the grant "Concurso Nacional de Asignación de Tiempo de Buque ASG-61 Cabo de Hor-

References

Bakun, A., & Nelson, C. S. (1991). The seasonal cycle of wind-stress curl in subtropical eastern boundary current regions. *Journal of Physical Oceanography*, *21*(12), 1815–1834. https://doi.org/10.1175/1520-0485(1991)021<1815:tscows>2.0.co;2

Bass, A. M., Munksgaard, N. C., O'Grady, D., Williams, M. J., Bostock, H. C., Rintoul, S. R., & Bird, M. I. (2014). Continuous shipboard measurements of oceanic $\delta^{18}O$, δD and $\delta^{13}C_{DIC}$ along a transect from New Zealand to Antarctica using cavity ring-down isotope spectrometry. *Journal of Marine Systems*, *137*, 21–27. https://doi.org/10.1016/j.jmarsys.2014.04.003

Bemis, B. E., Spero, H. J., Bijma, J., & Lea, D. W. (1998). Reevaluation of the oxygen isotopic composition of planktonic foraminifera: Experimental results and revised paleotemperature equations. *Paleoceanography*, *13*(2), 150–160. https://doi.org/10.1029/98pa00070

Benway, H. M., & Mix, A. C. (2004). Oxygen isotopes, upper-ocean salinity, and precipitation sources in the eastern tropical Pacific. *Earth and Planetary Science Letters*, *224*(3–4), 493–507. https://doi.org/10.1016/j.epsl.2004.05.014

Bigg, G. R., & Rohling, E. J. (2000). An oxygen isotope data set for marine waters. *Journal of Geophysical Research: Oceans*, *105*(C4), 8527–8535. https://doi.org/10.1029/2000jc900005

Bostock, H. C., Fletcher, S. E. M., & Williams, M. J. M. (2013). Estimating carbonate parameters from hydrographic data for the intermediate and deep waters of the Southern Hemisphere oceans. *Biogeosciences*, *10*(10), 6199–6213. https://doi.org/10.5194/bg-10-6199-2013

Bostock, H. C., Opdyke, B. N., & Williams, M. J. (2010). Characterising the intermediate depth waters of the Pacific Ocean using $\delta^{13}C$ and other geochemical tracers. *Deep Sea Research Part I: Oceanographic Research Papers*, *57*(7), 847–859. https://doi.org/10.1016/j.dsr.2010.04.005

Brand, W. A., Coplen, T. B., Vogl, J., Rosner, M., & Prohaska, T. (2014). Assessment of international reference materials for isotope-ratio analysis (IUPAC technical report). *Pure and Applied Chemistry*, *86*(3), 425–467. https://doi.org/10.1515/pac-2013-1023

Broecker, W. S., & Maier-Reimer, E. (1992). The influence of air and sea exchange on the carbon isotope distribution in the sea. *Global Biogeochemical Cycles*, *6*(3), 315–320. https://doi.org/10.1029/92gb01672

Caniupán, M., Lamy, F., Lange, C. B., Kaiser, J., Arz, H., Kilian, R., et al. (2011). Millennial-scale sea surface temperature and Patagonian Ice Sheet changes off southernmost Chile (53°S) over the past ~60 kyr. *Paleoceanography*, *26*(3). https://doi.org/10.1029/2010pa002049

Castillo, A., Valdés, J., Sifeddine, A., Reyss, J. L., Bouloubassi, I., & Ortlieb, L. (2017). Changes in biological productivity and ocean-climatic fluctuations during the last ~1.5 kyr in the Humboldt ecosystem off northern Chile (27°S): A multiproxy approach. *Palaeogeography, Palaeoclimatology, Palaeoecology*, *485*, 798–815. https://doi.org/10.1016/j.palaeo.2017.07.038

Charles, C. D., & Fairbanks, R. G. (1990). Glacial to interglacial changes in the isotopic gradients of southern ocean surface water. In U. Bleil, & J. Thiede, (Eds.), *Geological history of the polar oceans: Arctic versus Antarctic* (pp. 519–538). Kluwer Academic Publishers. https://doi.org/10.1007/978-94-009-2029-3_30

Charles, C. D., Wright, J. D., & Fairbanks, R. G. (1993). Thermodynamic influences on the marine carbon isotope record. *Paleoceanography*, *8*(6), 691–697. https://doi.org/10.1029/93pa01803

Chavez, F. P., & Messié, M. (2009). A comparison of eastern boundary upwelling ecosystems. *Progress in Oceanography*, *83*(1–4), 80–96. https://doi.org/10.1016/j.pocean.2009.07.032

Codispoti, L. A., & Christensen, J. P. (1985). Nitrification, denitrification and nitrous oxide cycling in the eastern tropical South Pacific Ocean. *Marine Chemistry*, *16*(4), 277–300. https://doi.org/10.1016/0304-4203(85)90051-9

Conroy, J. L., Cobb, K. M., Lynch-Stieglitz, J., & Polissar, P. J. (2014). Constraints on the salinity–oxygen isotope relationship in the central tropical Pacific Ocean. *Marine Chemistry*, *161*, 26–33. https://doi.org/10.1016/j.marchem.2014.02.001

Conroy, J. L., Cobb, K. M., & Noone, D. (2013). Comparison of precipitation isotope variability across the tropical Pacific in observations and SWING2 model simulations. *Journal of Geophysical Research: Atmospheres*, *118*(11), 5867–5892. https://doi.org/10.1002/jgrd.50412

Conroy, J. L., Thompson, D. M., Cobb, K. M., Noone, D., Rea, S., & LeGrande, A. N. (2017). Spatiotemporal variability in the $\delta^{18}O$-salinity relationship of seawater across the tropical Pacific Ocean. *Paleoceanography*, *32*(5), 484–497. https://doi.org/10.1002/2016pa003073

Cornejo D'Ottone, M., Bravo, L., Ramos, M., Pizarro, J., Karstensen, G.-M., Correa-Ramirez, M., et al. (2016). Biogeochemical characteristics of a long-lived anticyclonic eddy in the eastern South Pacific Ocean. *Biogeosciences*, *13*, 2971–2979. https://doi.org/10.5194/bg-13-2971-2016

Craig, H., & Gordon, L. (1965). Deuterium and $\delta^{18}O$ variations in the ocean and the marine atmosphere. In E. Ongiorgi (Ed.), *Stable isotopes in oceanographic studies and paleotemperatures*. (pp. 9–130). Laboratorio di Geologia Nucleare.

Czeschel, R., Schütte, F., Weller, R. A., & Stramma, L. (2018). Transport, properties, and life cycles of mesoscale eddies in the eastern tropical South Pacific. *Ocean Science*, *14*(4), 731–750. https://doi.org/10.5194/os-14-731-2018

Daneri, G., Dellarossa, V., Quiñones, R., Jacob, B., Montero, P., & Ulloa, O. (2000). Primary production and community respiration in the Humboldt Current System off Chile and associated oceanic areas. *Marine Ecology Progress Series*, *197*, 41–49. https://doi.org/10.3354/meps197041

Dávila, P. M., Figueroa, D., & Müller, E. (2002). Freshwater input into the coastal ocean and its relation with the salinity distribution off austral Chile (35–55°S). *Continental Shelf Research*, *22*(3), 521–534. https://doi.org/10.1016/s0278-4343(01)00072-3

De Pol-Holz, R., Ulloa, O., Dezileau, L., Kaiser, J., Lamy, F., & Hebbeln, D. (2006). Melting of the Patagonian ice Sheet and deglacial perturbations of the nitrogen cycle in the Eastern South Pacific. *Geophysical Research Letters*, *33*(4). https://doi.org/10.1029/2005gl024477

De Pol-Holz, R., Ulloa, O., Lamy, F., Dezileau, L., Sabatier, P., & Hebbeln, D. (2007). Late Quaternary variability of sedimentary nitrogen isotopes in the eastern South Pacific Ocean. *Paleoceanography*, *22*(2). https://doi.org/10.1029/2006pa001308

Deutsch, C., Brix, H., Ito, T., Frenzel, H., & Thompson, L. (2011). Climate-forced variability of ocean hypoxia. *Science*, *333*(6040), 336–339. https://doi.org/10.1126/science.1202422

DeVries, T., & Holzer, M. (2019). Radiocarbon and helium isotope constraints on deep ocean ventilation and mantle-3He sources. *Journal of Geophysical Research: Oceans*, *124*(5), 3036–3057. https://doi.org/10.1029/2018JC014716

DeVries, T., & Primeau, F. (2011). Dynamically and observationally constrained estimates of water-mass distributions and ages in the global ocean. *Journal of Physical Oceanography*, *41*(12), 2381–2401. https://doi.org/10.1175/JPO-D-10-05011.1

Druffel, E. R. M., & Griffin, S. (2015). Radiocarbon in dissolved organic carbon of the south Pacific Ocean. *Geophysical Research Letters*, *42*(10), 4096–4101. https://doi.org/10.1002/2015gl063764

nos" AUB180003, FONDECyT grants 11161091 (DN), 1180954 (CF), and the COPAS Sur-Austral Center (CONICYT PIA APOYO CCTE AFB170006). Sampling at Time-Series station 18 off Concepción during 2015 was funded by several FONDECYT/ANID grants from researchers at the Department of Oceanography and Research Line 5 of COPAS Sur-Austral (UdeC). ANID—Chile National Competition for ship time (AUB 150006/12806) financed the expedition LowpHOX organized by the Millennium Institute of Oceanography (IMO). The expedition Crio1218 was financed by the PPR 137 titled "Proyecto de Estudio Integrado del Afloramiento Costero Frente a Perú" and sponsored by IMARPE-Perú. Additional funding was provided by the ANID—Millennium Science Initiative Program—NCN19_153 (Millennium Nucleus UPWELL), ANID/FONDAP (CR)2 15110009 (LF and EMG), FONDECYT Grant 1210171 (CAV), ANID/FONDAP IDEAL 15150003 (CBL), and the Millennium Institute of Oceanography (IMO, ICN12_019). Dharma A. Reyes-Macaya was supported by Becas Chile (17342817-0), DAAD (57144001) and FARGO project (FAte of ocean oxygenation in a waRminG wOrld, UKRI). We dedicate this article to the memory of Nelson Silva, founder of the Chilean Oceanographic program CIMAR and pioneer in the study of water masses of the SEP.

Eide, M., Olsen, A., Ninnemann, U. S., & Eldevik, T. (2017). A global estimate of the full oceanic 13C Suess effect since the preindustrial. *Global Biogeochemical Cycles*, *31*(3), 492–514. https://doi.org/10.1002/2016GB005472

Epstein, S., Buchsbaum, R., Lowenstam, H. A., & Urey, H. C. (1953). Revised carbonate-water isotopic temperature scale. *Geological Society of America Bulletin*, *64*(11), 13152. https://doi.org/10.1130/0016-7606(1953)64[1315:rcits]2.0.co;2

Epstein, S., & Mayeda, T. (1953). Variation of ^{18}O content of waters from natural sources. *Geochimica et Cosmochimica Acta*, *4*(5), 213–224. https://doi.org/10.1016/0016-7037(53)90051-9

Fairbanks, R. G. (1989). A 17,000-year glacio-eustatic sea level record: Influence of glacial melting rates on the younger Dryas event and deep-ocean circulation. *Nature*, *342*(6250), 637–642. https://doi.org/10.1038/342637a0

Farías, L., Paulmier, A., & Gallegos, M. (2007). Nitrous oxide and N-nutrient cycling in the oxygen minimum zone off northern Chile. *Deep Sea Research Part I: Oceanographic Research Papers*, *54*(2), 164–180. https://doi.org/10.1016/j.dsr.2006.11.003

Farías, L., & Troncoso, M. (2021). *Extreme zonal and vertical gradients of nutrients and greenhouse gases in the subtropical Eastern South Pacific basin* [Data set]. PANGAEA. https://doi.org/10.1594/PANGAEA.933734

Ferdelman, T. G., Klockgether, G., Downes, P., & Lavik, G. (2019). *Nutrient Data from CTD Nisken Bottles from Sonne Expedition SO-245 "UltraPac"* [Data set]. PANGAEA. https://doi.org/10.1594/PANGAEA.899228

Fiedler, P. C., & Talley, L. D. (2006). Hydrography of the eastern tropical Pacific: A review. *Progress in Oceanography*, *69*(2–4), 143–180. https://doi.org/10.1016/j.pocean.2006.03.008

Figueroa, D., & Moffat, C. (2000). On the influence of topography in the induction of coastal upwelling along the Chilean Coast. *Geophysical Research Letters*, *27*(23), 3905–3908. https://doi.org/10.1029/1999gl011302

Garcia, H. E., Boyer, T. P., Locarnini, R. A., Antonov, J. I., Mishonov, A. V., Baranova, O. K., et al. (2014). *World Ocean Atlas 2013. Dissolved oxygen, apparent oxygen utilization, and oxygen saturation* (Vol. 3). NOAA Atlas NESDIS. Retrieved from https://repository.library.noaa.gov/view/noaa/14849

Graco, M., Ledesma, J., Flores, G., & Giron, M. (2007). Nutrientes, oxígeno y procesos biogeoquímicos en el sistema de surgencias de la corriente de Humboldt frente a Perú. Implicancias para los Recursos Costeros y su Manejo. *Revista Peruana de Biologia*, *14*(1), 117–128.

Graco, M. I., Ledesma, J., Flores, G., & Girón, M. (2013). Nutrientes, oxígeno y procesos biogeoquímicos en el sistema de surgencias de la corriente de Humboldt frente a Perú. *Revista Peruana de Biologia*, *14*(1). https://doi.org/10.15381/rpb.v14i1.2165

Grados, C., Chaigneau, A., Echevin, V., & Dominguez, N. (2018). Upper ocean hydrology of the Northern Humboldt Current System at seasonal, interannual and interdecadal scales. *Progress in Oceanography*, *165*, 123–144. https://doi.org/10.1016/j.pocean.2018.05.005

Gruber, N., Keeling, C. D., Bacastow, R. B., Guenther, P. R., Lueker, T. J., Wahlen, M., et al. (1999). Spatiotemporal patterns of carbon-13 in the global surface oceans and the oceanic Suess effect. *Global Biogeochemical Cycles*, *13*(2), 307–335. https://doi.org/10.1029/1999GB900019

Haddam, N. A., Michel, E., Siani, G., Licari, L., & Dewilde, F. (2020). Ventilation and expansion of intermediate and deep waters in the Southeast Pacific during the last termination. *Paleoceanography and Paleoclimatology*, *35*(7). https://doi.org/10.1029/2019pa003743

Haddam, N. A., Siani, G., Michel, E., Kaiser, J., Lamy, F., Duchamp-Alphonse, S., et al. (2018). Changes in latitudinal sea surface temperature gradients along the Southern Chilean margin since the last glacial. *Quaternary Science Reviews*, *194*, 62–76. https://doi.org/10.1016/j.quascirev.2018.06.023

Halpin, P. M., Strub, P. T., Peterson, W. T., & Baumgartner, T. R. (2004). An overview of interactions among oceanography, marine ecosystems, climatic and human disruptions along the eastern margins of the Pacific Ocean. *Revista Chilena de Historia Natural*, *77*(3). https://doi.org/10.4067/s0716-078x2004000300002

Hamersley, M. R., Lavik, G., Woebken, D., Rattray, J. E., Lam, P., Hopmans, E. C., et al. (2007). Anaerobic ammonium oxidation in the Peruvian oxygen minimum zone. *Limnology & Oceanography*, *52*(3), 923–933. https://doi.org/10.4319/lo.2007.52.3.0923

Hanawa, K., & Talley, L. (2001). Chapter 5.4, mode waters. *International Geophysics Ocean Circulation and Climate—Observing and Modelling the Global Ocean*, *77*, 373–386. https://doi.org/10.1016/s0074-6142(01)80129-7

Hartin, C. A., Fine, R. A., Sloyan, B. M., Talley, L. D., Chereskin, T. K., & Happell, J. (2011). Formation rates of Subantarctic mode water and Antarctic intermediate water within the South Pacific. *Deep Sea Research Part I: Oceanographic Research Papers*, *58*(5), 524–534. https://doi.org/10.1016/j.dsr.2011.02.010

Hebbeln, D., Marchant, M., Freudenthal, T., & Wefer, G. (2000). Surface sediment distribution along the Chilean continental slope related to upwelling and productivity. *Marine Geology*, *164*(3–4), 119–137. https://doi.org/10.1016/s0025-3227(99)00129-2

Hernández-Vaca, F., Schneider, W., & Garcés-Vargas, J. (2017). Contribution of Ekman pumping to the changes in properties and volume of the Eastern South Pacific intermediate water. *Gayana*, *81*(2), 52–63. https://doi.org/10.4067/s0717-65382017000200052

Holmes, R. M., Peterson, B. J., Deegan, L. A., Hughes, J. E., & Fry, B. (2000). Nitrogen biogeochemistry in the oigohaline zone of A New England Estuary. *Ecology*, *81*(2), 4162–4432. https://doi.org/10.1890/0012-9658(2000)081[0416:nbitoz]2.0.co;2

Hormazabal, S., Combes, V., Morales, C. E., Correa–Ramirez, M. A., Di Lorenzo, E., & Nuñez, S. (2013). Intrathermocline eddies in the coastal transition zone off central Chile (31–41 S). *Journal of Geophysical Research: Oceans*, *118*, 4811–4821. https://doi.org/10.1002/jgrc.20337

Hupe, A., & Karstensen, J. (2000). Redfield stoichiometry in Arabian Sea subsurface waters. *Global Biogeochemical Cycles*, *14*(1), 357–372. https://doi.org/10.1029/1999gb900077

IAEA. (2017). *Reference sheet for international measurement standards*.

Ishimura, T., Tsunogai, U., Hasegawa, S., Nakagawa, F., Oi, T., Kitazato, H., et al. (2012). Variation in stable carbon and oxygen isotopes of individual benthic foraminifera: Tracers for quantifying the vital effect. *Biogeosciences Discussions*, *9*(5), 4353–4367. https://doi.org/10.5194/bg-9-4353-2012

Karstensen, J., & Tomczak, M. (1998). Age determination of mixed water masses using CFC and oxygen data. *Journal of Geophysical Research: Oceans*, *103*(C9), 18599–18609. https://doi.org/10.1029/98jc00889

Karstensen, J., & Ulloa, O. (2009). Peru–Chile current system In J. H. Steele, S. A. Thorpe, & K. K. Turekian, (Eds.), *Encyclopedia of Ocean Sciences*. (pp. 385–392). Academic Press. https://doi.org/10.1016/b978-012374473-9.00599-3

Keeling, C. D. (1979). The suess effect: 13Carbon-14Carbon interrelations. *Environment International*, *2*(4–6), 229–300. https://doi.org/10.1016/0160-4120(79)90005-9

Kessler, W. S., & Gourdeau, L. (2006). Wind-driven zonal jets in the south Pacific Ocean. *Geophysical Research Letters*, *33*(3). https://doi.org/10.1029/2005gl025084

Khatiwala, S. P., Fairbanks, R. G., & Houghton, R. W. (1999). Freshwater sources to the coastal ocean off northeastern North America: Evidence from $H_2{}^{18}O/H_2{}^{16}O$. *Journal of Geophysical Research: Oceans*, *104*(C8), 18241–18255. https://doi.org/10.1029/1999jc900155

Koshlyakov, M., & Tarakanov, R. Y. (2004). Pacific deep water in the southern ocean. *Oceanology*, *44*(3), 299–314.

Kroopnick, P. (1985). The distribution of ^{13}C of ΣCO_2 in the world oceans. *Deep Sea Research Part I: Oceanographic Research Papers*, *32*(1), 57–84. https://doi.org/10.1016/0198-0149(85)90017-2

Kumamoto, Y., Murata, A., Watanabe, S., & Fukasawa, M. (2011). Temporal and spatial variations in bomb-produced radiocarbon along BEAGLE2003 lines—Revisits of WHP P06, A10, and I03/I04 in the Southern Hemisphere Oceans. *Progress in Oceanography*, *89*(1–4), 49–60. https://doi.org/10.1016/j.pocean.2010.12.007

Lavik, G., & Krahmann, G. (2016). *Hydrochemistry of water samples during METEOR cruise M93* [Data set]. PANGAEA. https://doi.org/10.1594/PANGAEA.862055

LeGrande, A. N., & Schmidt, G. A. (2006). Global gridded data set of the oxygen isotopic composition in seawater. *Geophysical Research Letters*, *33*(12). https://doi.org/10.1029/2006gl026011

Letelier, J., Pizarro, O., & Nuñez, S. (2009). Seasonal variability of coastal upwelling and the upwelling front off central Chile. *Journal of Geophysical Research*, *114*(C12). https://doi.org/10.1029/2008jc005171

Leth, O., Shaffer, G., & Ulloa, O. (2004). Hydrography of the Eastern South Pacific Ocean: Results from the Sonne 102 cruise, May–June 1995. *Deep Sea Research Part II: Topical Studies in Oceanography*, *51*(20–21), 2349–2369. https://doi.org/10.1016/j.dsr2.2004.08.009

Llanillo, P. J., Karstensen, J., Pelegrí, J. L., & Stramma, L. (2013). Physical and biogeochemical forcing of oxygen and nitrate changes during El Niño/El Viejo and La Niña/La Vieja upper-ocean phases in the tropical eastern South Pacific along 86 °W. *Biogeosciences*, *10*(10), 6339–6355. https://doi.org/10.5194/bg-10-6339-2013

Llanillo, P. J., Pelegrí, J. L., Duarte, C. M., Emelianov, M., Gassen, M., Gourrion, A., & Rodriguez-Santana, A. (2012). Meridional and zonal changes in water properties along the continental slope off central and northern Chile. *Ciencias Marinas*, *38*(1B), 307–332. https://doi.org/10.7773/cm.v38i1b.1814

Llanillo, P. J., Pelegrí, J. L., Talley, L. D., Peña-Izquierdo, J., & Cordero, R. R. (2018). Oxygen pathways and budget for the Eastern South Pacific oxygen minimum zone. *Journal of Geophysical Research: Oceans*, *123*(3), 1722–1744. https://doi.org/10.1002/2017jc013509

Luyten, J. R., Pedlosky, J., & Stommel, H. (1983). The ventilated thermocline. *Journal of Physical Oceanography*, *13*(2), 292–309. https://doi.org/10.1175/1520-0485(1983)013<0292:tvt>2.0.co;2

Lynch-Stieglitz, J., Curry, W. B., & Slowey, N. (1999). A geostrophic transport estimate for the Florida Current from the oxygen isotope composition of benthic foraminifera. *Paleoceanography*, *14*(3), 360–373. https://doi.org/10.1029/1999pa900001

Lynch-Stieglitz, J., Stocker, T. F., Broecker, W. S., & Fairbanks, R. G. (1995). The influence of air-sea exchange on the isotopic composition of oceanic carbon: Observations and modeling. *Global Biogeochemical Cycles*, *9*(4), 653–665. https://doi.org/10.1029/95gb02574

Macdonald, R. W., Carmack, E. C., Mclaughlin, F. A., Falkner, K. K., & Swift, J. H. (1999). Connections among ice, runoff and atmospheric forcing in the Beaufort Gyre. *Geophysical Research Letters*, *26*(15), 2223–2226. https://doi.org/10.1029/1999gl900508

Mackensen, A. (2001). Oxygen and carbon stable isotope tracers of Weddell sea water masses: New data and some paleoceanographic implications. *Deep Sea Research Part I: Oceanographic Research Papers*, *48*(6), 1401–1422. https://doi.org/10.1016/s0967-0637(00)00093-5

Mackensen, A., Hubberten, H. W., Bickert, T., Fischer, G., & Fütterer, D. K. (1993). The $\delta^{13}C$ in benthic foraminiferal tests of Fontbotia wuellerstorfi (Schwager) relative to the $\delta^{13}C$ of dissolved inorganic carbon in southern ocean deep water: Implications for glacial ocean circulation models. *Paleoceanography*, *8*(5), 587–610. https://doi.org/10.1029/93PA01291

Marchitto, T., Curry, W., Lynch-Stieglitz, J., Bryan, S., Cobb, K., & Lund, D. (2014). Improved oxygen isotope temperature calibrations for cosmopolitan benthic foraminifera. *Geochimica et Cosmochimica Acta*, *130*, 1–11. https://doi.org/10.1016/j.gca.2013.12.034

Martinez-Fontaine, C., De Pol-Holz, R., Michael, E., Martinez-Mendez, G., DeVries, T., Stott, L., et al. (2019). Ventilation of the deep–ocean carbon reservoir during the last deglaciation: Results from the Southeast Pacific. *Paleoceanography*, *34*(12), 2080–2097. https://doi.org/10.1029/2019PA003613

Martínez-Méndez, G., Hebbeln, D., Mohtadi, M., Lamy, F., Pol-Holz, R. D., Reyes-Macaya, D., & Freudenthal, T. (2013a). Changes in the advection of Antarctic Intermediate Water to the northern Chilean coast during the last 970 kyr. *Paleoceanography*, *28*(4), 607–618. https://doi.org/10.1002/palo.20047

Martínez Méndez, G., Hebbeln, D., Mohtadi, M., Lamy, F., De Pol-Holz, R., Reyes-Macaya, D., & Freudenthal, T. (2013b). *Water sample measurements of sediment core GeoB15011-1* [Data set]. PANGAEA. https://doi.org/10.1594/PANGAEA.820557

Martínez Méndez, G., Hebbeln, D., Mohtadi, M., Lamy, F., De Pol-Holz, R., Reyes-Macaya, D., & Freudenthal, T. (2013c). *Water sample measurements of sediment core GeoB15007-1* [Data set]. PANGAEA. https://doi.org/10.1594/PANGAEA.820538

Martínez Méndez, G., Hebbeln, D., Mohtadi, M., Lamy, F., De Pol-Holz, R., Reyes-Macaya, D., & Freudenthal, T. (2013d). *Water sample measurements of sediment core GeoB15024-1* [Data set]. PANGAEA. https://doi.org/10.1594/PANGAEA.820564

Martínez Méndez, G., Hebbeln, D., Mohtadi, M., Lamy, F., De Pol-Holz, R., Reyes-Macaya, D., & Freudenthal, T. (2013e). *Water sample measurements of sediment core GeoB15004-1* [Data set]. PANGAEA. https://doi.org/10.1594/PANGAEA.820536

Masotti, I., Aparicio-Rizzo, P., Yevenes, M. A., Garreaud, R., Belmar, L., & Farías, L. (2018). The influence of river discharge on nutrient export and phytoplankton biomass off the Central Chile coast (33°–37°S): Seasonal cycle and interannual variability. *Frontiers in Marine Science*, *5*. https://doi.org/10.3389/fmars.2018.00423

McCartney, M. S. (1977). Subantarctic mode water. In M. Angel (Ed.), *A voyage of discovery, supplement to deep–sea research George Deacon 70th anniversary volume* (pp. 103–119). Pergamon.

McCorkle, D. C., & Keigwin, L. D. (1994). Depth profiles of $\delta^{13}C$ in bottom water and core top C. wuellerstorfi on the Ontong Java Plateau and Emperor Seamounts. *Paleoceanography*, *9*(2), 197–208. https://doi.org/10.1029/93PA03271

McNeil, B. I., Matear, R. J., & Tilbrook, B. (2001). Does carbon 13 track anthropogenic CO_2 in the Southern Ocean? *Global Biogeochemical Cycles*, *15*, 597–613. https://doi.org/10.1029/2000GB001352

Meredith, M. P., Heywood, K. J., Frew, R. D., & Dennis, P. F. (1999). Formation and circulation of the water masses between the southern Indian Ocean and Antarctica: Results from $\delta^{18}O$. *Journal of Marine Research*, *57*(3), 449–470. https://doi.org/10.1357/002224099764805156

Mikalsen, G., & Sejrup, H. (2000). Oxygen isotope composition of fjord and river water in the Sognefjorden Drainage area, western Norway. Implications for Paleoclimate studies, Estuarine. *Coastal and Shelf Science*, *50*(4), 441–448. https://doi.org/10.1006/ecss.1999.0581

Mohtadi, M., Hebbeln, D., & Marchant, M. (2005). Upwelling and productivity along the Peru–Chile Current derived from faunal and isotopic compositions of planktic foraminifera in surface sediments. *Marine Geology*, *206*, 107–126. https://doi.org/10.1016/j.margeo.2005.01.008

Mohtadi, M., Rossel, P., Lange, C. B., Pantoja, S., Böning, P., Repeta, D. J., et al. (2008). Deglacial pattern of circulation and marine productivity in the upwelling region off central-south Chile. *Earth and Planetary Science Letters*, *272*(1–2), 221–230. https://doi.org/10.1016/j.epsl.2008.04.043

Montecino, V., & Lange, C. (2009). The Humboldt Current System: Ecosystem components and processes, fisheries, and sediment studies. *Progress in Oceanography*, *83*(1–4), 65–79. https://doi.org/10.1016/j.pocean.2009.07.041

Montecino, V., Paredes, M. A., Paolini, P., & Rutllant, J. (2006). Revisiting chlorophyll data along the coast in north-central Chile, considering multiscale environmental variability. *Revista Chilena de Historia Natural*, *79*(2). https://doi.org/10.4067/s0716-078x2006000200007

Montero, P., Daneri, G., Cuevas, L. A., González, H. E., Jacob, B., Lizárraga, L., & Menschel, E. (2007). Productivity cycles in the coastal upwelling area off Concepción: The importance of diatoms and bacterioplankton in the organic carbon flux. *Progress in Oceanography*, *75*(3), 518–530. https://doi.org/10.1016/j.pocean.2007.08.013

Morales, C. E., Blanco, J. L., Braun, M., Reyes, H., & Silva, N. (1996). Chlorophyll-a distribution and associated oceanographic conditions in the upwelling region off northern Chile during the winter and spring 1993. *Deep Sea Research Part I: Oceanographic Research Papers*, *43*(3), 267–289. https://doi.org/10.1016/0967-0637(96)00015-5

Morales, C. E., Braun, M., Reyes, H., Blanco, J. L., & Davies, A. G. (1996). Anchovy larval distribution in the coastal zone off northern Chile: The effect of low dissolved oxygen concentrations and of a cold-warm sequence (1990-95). *Investigaciones Marinas*, *24*. https://doi.org/10.4067/s0717-71781996002400007

Morales, C. E., Hormazábal, S. E., & Blanco, J. (1999). Interannual variability in the mesoscale distribution of the depth of the upper boundary of the oxygen minimum layer off northern Chile (18–24S): Implications for the pelagic system and biogeochemical cycling. *Journal of Marine Research*, *57*(6), 909–932. https://doi.org/10.1357/002224099321514097

Morales, C. E., Hormazábal, S. E., Correa-Ramirez, M., Pizarro, O., Silva, N., Fernandez, C., et al. (2012). Mesoscale variability and nutrient–phytoplankton distributions off central-southern Chile during the upwelling season: The influence of mesoscale eddies. *Progress in Oceanography*, *104*, 17–29.

Naqvi, S. W. A., Bange, H. W., Farias, L., Monteiro, P. M. S., Scranton, M. I., & Zhang, J. (2010). Marine hypoxia/anoxia as a source of CH_4 and NO. *Biogeosciences*, *7*, 2159–2190. https://doi.org/10.5194/bg-7-2159-2010

Narváez, D. A., Vargas, C. A., Cuevas, L. A., García-Loyola, S. A., Lara, C., Segura, C., et al. (2019). Dominant scales of subtidal variability in coastal hydrography of the Northern Chilean Patagonia. *Journal of Marine Systems*, *193*, 59–73. https://doi.org/10.1016/j.jmarsys.2018.12.008

Nürnberg, D., Böschen, T., Doering, K., Mollier-Vogel, E., Raddatz, J., & Schneider, R. (2015). Sea surface and subsurface circulation dynamics off equatorial Peru during the last ~17kyr. *Paleoceanography*, *30*(7), 984–999. https://doi.org/10.1002/2014pa002706

O'Neil, J. R., Clayton, R. N., & Mayeda, T. K. (1969). Oxygen isotope fractionation in divalent metal carbonates. *The Journal of Chemical Physics*, *51*(12), 5547–5558. https://doi.org/10.1063/1.1671982

Oppo, D. W., & Fairbanks, R. G. (1989). Carbon isotope composition of tropical surface water during the past 22,000 years. *Paleoceanography*, *4*(4), 333–351. https://doi.org/10.1029/pa004i004p00333

Pantoja, S., Iriarte, J. L., & Daneri, G. (2011). Oceanography of the Chilean Patagonia. *Continental Shelf Research*, *31*(3–4), 149–153. https://doi.org/10.1016/j.csr.2010.10.013

Pearson, P. N. (2012). Oxygen isotopes in foraminifera: Overview and historical review. *Paleontological Society Papers*, *18*, 1–38. https://doi.org/10.1017/S1089332600002539

Piola, A. R., & Gordon, A. L. (1989). Intermediate waters in the southwest south Atlantic. *Deep Sea Research Part I: Oceanographic Research Papers*, *36*(1), 1–16. https://doi.org/10.1016/0198-0149(89)90015-0

Poole, R., & Tomczak, M. (1999). Optimum multiparameter analysis of the water mass structure in the Atlantic Ocean thermocline. *Deep Sea Research Part I: Oceanographic Research Papers*, *46*(11), 1895–1921. https://doi.org/10.1016/s0967-0637(99)00025-4

Quay, P., Sonnerup, R., Westby, T., Stutsman, J., & Mcnichol, A. (2003). Changes in the $^{13}C/^{12}C$ of dissolved inorganic carbon in the ocean as a tracer of anthropogenic CO_2 uptake. *Global Biogeochemical Cycles*, *17*(1). https://doi.org/10.1029/2001gb001817

Rojas, R., & Silva, N. (1996). *Atlas oceanográfico de Chile (18º 21' S a 50º 00' S), volumen 1*. Servicio Hidrográfico y Oceanográfico de la Armada de Chile.

Rutllant, J., & Montecino, V. (2002). Multiscale upwelling forcing cycles and biological response off north-central Chile. *Revista Chilena de Historia Natural*, *75*(1), 217–231. https://doi.org/10.4067/S0716-078X2002000100020

Sansone, F. J., Popp, B. N., Gasc, A., Graham, A. W., & Rust, T. M. (2001). Highly elevated methane in the eastern tropical North Pacific and associated isotopically enriched fluxes to the atmosphere. *Geophysical Research Letters*, *28*(24), 4567–4570. https://doi.org/10.1029/2001gl013460

Schlitzer, R. (2021). *Ocean Data View*. Retrieved from https://odv.awi.de

Schmidt, G. A. (1998). Oxygen-18 variations in a global ocean model. *Geophysical Research Letters*, *25*(8), 1201–1204. https://doi.org/10.1029/98GL50866

Schmidt, G. A. (1999). Forward modeling of carbonate proxy data from planktonic foraminifera using oxygen isotope tracers in a global ocean model. *Paleoceanography*, *14*(4), 482–497. https://doi.org/10.1029/1999pa900025

Schmidt, G. A. (2009). Error analysis of paleosalinity calculations. *Paleoceanography*, *14*(3), 422–429. https://doi.org/10.1029/1999PA900008

Schmittner, A., Bostock, H. C., Cartapanis, O., Curry, W. B., Filipsson, H. L., Galbraith, E. D., et al. (2017). Calibration of the carbon isotope composition ($\delta^{13}C$) of benthic foraminifera. *Paleoceanography*, *32*, 512–530. https://doi.org/10.1002/2016PA003072

Schneider, W., Fuenzalida, R., Rodríguez-Rubio, E., & Bravo, L. (2003). Characteristics and formation of Eastern South Pacific intermediate water. *Geophysical Research Letters*, *30*(11). https://doi.org/10.1029/2003gl017086

Shackleton, N. (1967). Oxygen isotope analyses and Pleistocene temperatures Re-assessed. *Nature*, *215*(5096), 15–17. https://doi.org/10.1038/215015a0

Shaffer, G., Salinas, S., Pizarro, O., Vega, A., & Hormazabal, S. (1995). Currents in the deep ocean off Chile (30°S). *Deep Sea Research Part I: Oceanographic Research Papers*, *42*(4), 425–436. https://doi.org/10.1016/0967-0637(95)99823-6

Siani, G., Michel, E., Pol-Holz, R. D., Devries, T., Lamy, F., Carel, M., et al. (2013). Carbon isotope records reveal precise timing of enhanced Southern Ocean upwelling during the last deglaciation. *Nature Communications*, *4*(1). https://doi.org/10.1038/ncomms3758

Silva, N., Calvete, C., & Sievers, H. A. (1997). Características oceanográficas físicas y químicas de canales australes chilenos entre Puerto Montt y laguna San Rafael (Crucero CIMAR-Fiordo 1). *Ciencia y Tecnología Marina*, *20*, 23–106

Silva, N., & Neshyba, S. (1979/1980). Masas de agua y circulación geostrófica frente a la costa de Chile Austral. *Serie científica - Instituto Antártico Chileno*, *25–26*, 5–32.

Silva, N., Rojas, N., & Fedele, A. (2009). Water masses in the Humboldt Current System: Properties, distribution, and the nitrate deficit as a chemical water mass tracer for Equatorial Subsurface Water off Chile. *Deep Sea Research Part II: Topical Studies in Oceanography*, *56*(16), 1004–1020. https://doi.org/10.1016/j.dsr2.2008.12.013

Spero, H. (1992). Do planktic foraminifera accurately record shifts in the carbon isotopic composition of seawater sigma-CO_2 *Marine Micropaleontology*, *19*(4), 275–285. https://doi.org/10.1016/0377-8398(92)90033-G

Spero, H. J., Mielke, K. M., Kalve, E. M., Lea, D. W., & Pak, D. K. (2003). Multispecies approach to reconstructing eastern equatorial Pacific thermocline hydrography during the past 360 kyr. *Paleoceanography*, *18*(1). https://doi.org/10.1029/2002PA000814

Stramma, L., Bange, H. W., Czeschel, R., Lorenzo, A., & Frank, M. (2013). On the role of mesoscale eddies for the biological productivity and biogeochemistry in the eastern tropical Pacific Ocean off Peru. *Biogeosciences*, *10*(11), 7293–7306. https://doi.org/10.5194/bg-10-7293-2013

Stramma, L., Johnson, G. C., Firing, E., & Schmidtko, S. (2010). Eastern Pacific oxygen minimum zones: Supply paths and multidecadal changes. *Journal of Geophysical Research*, *115*(C9). https://doi.org/10.1029/2009jc005976

Stramma, L., Peterson, R. G., & Tomczak, M. (1995). The South Pacific current. *Journal of Physical Oceanography*, *25*(1), 77–91. https://doi.org/10.1175/1520-0485(1995)025<0077:tspc>2.0.co;2

Strub, P., James, V., Montecino, V., Rutllant, J., & Blanco, J. (2019). Ocean circulation along the southern Chile transition region (38°–46°S): Mean, seasonal and interannual variability, with a focus on 2014-2016. *Progress in Oceanography*, *172*, 159–198. https://doi.org/10.1016/j.pocean.2019.01.004

Strub, P., Mesías, J., Montecino, V., & Rutllant, J. (1998). Coastal ocean circulation off western South America. In A. R. Robinson & K. H. Brink (Eds.), *The global coastal ocean the sea* (pp. 273–313). John Wiley.

Suess, H. E. (1955). Radiocarbon concentration in modern wood. *Science*, *122*(3166), 415–417.

Talley, L. (2013). Closure of the global overturning circulation through the Indian, Pacific, and southern oceans: Schematics and transports. *Oceanography*, *26*(1), 80–97. https://doi.org/10.5670/oceanog.2013.07

Tapia, R., Nuernberg, D., Ronge, T., & Tiedemann, R. (2015). Disparities in glacial advection of southern ocean intermediate water to the south Pacific Gyre. *Earth and Planetary Science Letters*, *410*, 152–164. https://doi.org/10.1016/j.epsl.2014.11.031

Tapia, R., Nürnberg, D., Ho, S. L., Lamy, F., Ullermann, J., Gersonde, R., & Tiedemann, R. (2019). Glacial differences of southern ocean intermediate waters in the central South Pacific. *Quaternary Science Reviews*, *208*, 105–117. https://doi.org/10.1016/j.quascirev.2019.01.016

Tenorio, S. (2021). *Mecanismos de Generación de Metano en la zona Fótica en sistemas marinos altamente productivos*. Master program in Oceanography Sciences at University of Concepcion.

Testa, J. M., Murphy, R. R., Brady, D. C., & Kemp, W. M. (2018). Nutrient and climate induced shifts in the phenology of linked biogeochemical cycles in a temperate estuary. *Frontiers in Marine Science*, *5*. https://doi.org/10.3389/fmars.2018.00114

Thamdrup, B., Dalsgaard, T., Mark-Jensen, M., Ulloa, O., Farias, L., & Escribano, R. (2006). Anaerobic ammonium oxidation in the oxygen-deficient water off northern Chile. *Limnology & Oceanography*, *51*(5), 2145–2156. https://doi.org/10.4319/lo.2006.51.5.2145

Tiwari, M., Nagoji, S. S., Kartik, T., Drishya, G., Parvathy, R., & Rajan, S. (2013). Oxygen isotope salinity relationships of discrete oceanic regions from India to Antarctica, surface hydrological processes. *Journal of Marine Systems*, *113*(114), 88–93. https://doi.org/10.1016/j.jmarsys.2013.01.001

Tomczak, M., & Large, D. G. (1989). Optimum multiparameter analysis of mixing in the thermocline of the eastern Indian Ocean. *Journal of Geophysical Research: Oceans*, *94*(C11), 16141–16149. https://doi.org/10.1029/JC094iC11p16141

Troncoso, M., Garcia, G., Verdugo, J., & Farías, L. (2018). Toward high-resolution vertical measurements of dissolved greenhouse gases (Nitrous Oxide and Methane) and nutrients in the eastern South Pacific. *Frontiers in Marine Science*, *5*. https://doi.org/10.3389/fmars.2018.00148

Tsuchiya, M., & Talley, L. D. (1998). A Pacific hydrographic section at 88°W: Water-property distribution. *Journal of Geophysical Research: Atmospheres*, *1031*(C6), 12899–12918. https://doi.org/10.1029/97JC03415

Ulloa, O., & Pantoja, S. (2009). The oxygen minimum zone of the eastern South Pacific. *Deep Sea Research Part II: Topical Studies in Oceanography*, *56*(16), 987–991. https://doi.org/10.1016/j.dsr2.2008.12.004

Urey, H. C. (1947). The thermodynamic properties of isotopic substances. *Journal of the Chemical Society*, *562*. https://doi.org/10.1039/jr9470000562

Vargas, C. A., Cantarero, S. I., Sepúlveda, J. A., Galán, A., De Pol Holz, R., Walker, B., et al. (2021). A source of isotopically light organic carbon in a low-pH anoxic marine zone. *Nature Communications*, *12*, 1604. https://doi.org/10.1038/s41467-021-21871-4

Vargas, C. A., Contreras, P. Y., Pérez, C. A., Sobarzo, M., Saldías, G. S., & Salisbury, J. (2016). Influences of riverine and upwelling waters on the coastal carbonate system off Central Chile and their ocean acidification implications. *Journal of Geophysical Research: Biogeoscioscience*s, *121*. https://doi.org/10.1002/2015JG003213

Vargas, C. A., Cuevas, L. A., Silva, N., González, H. E., De Pol-Holz, R., & Narváez, D. A. (2018). Influence of glacier melting and river discharges on the nutrient distribution and DIC recycling in the southern Chilean Patagonia. *Journal of Geophysical Research: Biogeosciences*, *123*(1), 256–270. https://doi.org/10.1002/2017jg003907

Vergara, O. A., Echevín, V., Sepúlveda, H. H., & Quiñones, R. A. (2017). Controlling factor of the seasonal variability of productivity in the southern Humboldt current system (30–40°S): A biophysical modeling approach. *Continental Shelf Research*, *148*, 89–103. https://doi.org/10.1016/j.csr.2017.08.013

Wang, Y., Zhang, H. R., Chai, F., & Yuan, Y. (2018). Impact of mesoscale eddies on chlorophyll variability off the coast of Chile. *PLoS One*, *13*(9), e0203598. https://doi.org/10.1371/journal.pone.0203598

Wooster, W. S., & Gilmartin, M. (1961). The Peru–Chile undercurrent. *Journal of Marine Research*, *19*, 97–122.

Wyrtki, K. (1973). Teleconnections in the equatorial Pacific Ocean. *Science*, *180*(4081), 66–68. https://doi.org/10.1126/science.180.4081.66

Zhang, Z., Wang, W., & Qiu, B. (2014). Oceanic mass transport by mesoscale eddies. *Science*, *345*(6194), 322–324. https://doi.org/10.1126/science.1252418

References From the Supporting Information

Armstrong, F. A. J. (1963). The determination of nitrate in water by ultra-violet spectrophotometry. *Analyst Chemistry*, *35*, 1292–1294.

Grasshoff, K., Ehrhardt, M., & Kremling, K. (1983). *Methods of seawater analysis* (2nd ed, p. 419). Verlag Chemie Weinhein.

Grasshoff, K., Kremling, K., & Ehrhardt (1999). *Methods of seawater analysis* (3rd ed). https://doi.org/10.1002/9783527613984

Murphy, J., & Riley, J.P. (1962). A modified single solution method for the determination of phosphate in natural waters. *Analytica Chimica Acta*, *27*, 31–36. https://doi.org/10.1016/S0003-2670(00)88444-5

Strickland, J. D. H., & Parsons, T. R. (1972). A practical hand-book of seawater analysis. *Fisheries Research Board of Canada Bulletin* (2nd ed., Vol. 157, p. 310).